การศึกษาการรู้จำภาพจอประสาทตาด้วยจอยท์ทรานส์ฟอร์มคอร์รีเลเตอร์โดยใช้ภาพแบบบีบอัด

พันตรีโกมินทร์ แก้วผลึก

วิทยานิพนธ์นี้เป็นส่วนหนึ่งของการศึกษาตามหลักสูตรปริญญาวิทยาศาสตรดุษฎีบัณฑิต
สาขาวิชาฟิสิกส์
มหาวิทยาลัยเทคโนโลยีสุรนารี
ปีการศึกษา 2557

STUDY OF RETINA RECOGNITION USING COMPRESSION-BASED JOINT TRANSFORM CORRELATOR

Komin Kaewphaluk

A Thesis submitted in Partial Fulfillment of the Requirements for the

Degree of Doctor of Philosophy in Physics

Suranaree University of Technology

Academic Year 2014

STUDY OF RETINA RECOGNITION USING COMPRESSION-BASED JOINT TRANSFORM CORRELATOR

Suranaree University of Technology has approved this thesis submitted in partial fulfillment of the requirements for the Degree of Doctor of Philosophy.

Thesis Examining Committee

_____

(Prof. Dr. Santi Maensiri)

Chairperson

_____

(Prof. Dr. Joewono Widjaja)

Member (Thesis Advisor)

_____

(Dr. Ubon Suripon)

Member

_____

(Prof. Dr. Yupeng Yan)

Member

_____

(Dr. Panomsak Meemon)

Member

_____ _____

(Prof. Dr. Sukit Limpijumnong) (Assoc. Prof. Dr. Prapun Manyum)

Vice Rector for Academic Affairs Dean of Institute of Science

and Innovation

โกมินทร์ แก้วผลึก : การศึกษาการรู้จำภาพจอประสาทตาด้วยจอยท์ทรานส์ฟอร์มคอร์รีเลเตอร์โดยใช้ภาพแบบบีบอัด (STUDY OF RETINA RECOGNITION USING COMPRESSION BASED-JOINT TRANSFORM CORRELATOR) อาจารย์ที่ปรึกษา : ศาสตราจารย์ ดร.ยูโวโน วิดจายา, 68 หน้า.

งานวิทยานิพนธ์นี้ได้นำเสนอและศึกษาผลการทดลองการรู้จำภาพจอประสาทตาด้วยจอยท์ทรานส์ฟอร์มคอร์รีเลเตอร์โดยใช้ภาพแบบบีบอัด การศึกษามุ่งเน้นไปที่ 2 หัวข้อหลัก หัวข้อแรกคือไม่ว่าจะเป็นสัญญาณรบกวนที่ภาพจอประสาทตาจะสามารถถูกขจัดโดยใช้การบีบอัดภาพแบบ JPEG ในขณะที่หัวข้อที่สองคือ การปรับปรุงการรู้จำภาพจอประสาทตาโดยวิธีการผสมผสานตัวกรองสัญญาณเวฟเล็ตเข้ากับจอยท์ทรานส์ฟอร์มคอร์รีเลเตอร์แบบบีบอัด ผลการทดลองแสดงให้เห็นว่า ประการแรก การขจัดสัญญาณรบกวนสามารถได้มาโดยการเลือกระดับการบีบอัดที่เหมาะสม เช่น สัญญาณรบกวนอย่างเข้มจะเหมาะสมกับระดับการบีบอัดน้อย ประการที่สอง การรู้จำภาพจอประสาทตาโดยวิธีการผสมผสานตัวกรองสัญญาณเวฟเล็ตให้ผลการรู้จำที่ดีขึ้นในทุกระดับของสัญญาณรบกวน ผลลัพธ์ที่ได้จากวิธีการดังกล่าวดีกว่าวิธีการจอยท์ทรานส์ฟอร์มคอร์รีเลเตอร์แบบธรรมดาสำหรับคุณภาพการบีบอัดทุกระดับ

สาขาวิชาฟิสิกส์ ลายมือชื่อนักศึกษา_____

ปีการศึกษา 2557 ลายมือชื่ออาจารย์ที่ปรึกษา_____

KOMIN KAEWPHALUK : STUDY OF RETINA RECOGNITION USING COMPRESSION-BASED JOINT TRANSFORM CORRELATOR. THESIS ADVISOR : PROF. JOEWONO WIDJAJA, Ph.D. 68 PP.

PATTERM RECOGNITION/JOINT TRANSFORM CORRELATOR/JPEG-COMPRESSION/WAVELET-BASED JOINT TRANSFORM CORRELATOR

Retina recognition by using compression-based joint transform correlator (CBJTC) has been proposed and experimentally studied. The study focused on 2 main topics. The first topic was whether noise corrupted retinal targets could be suppressed by using Electrically-Addressed Spatial Light Modulator (JPEG) image compression, while the second one was the improvement of retina recognition by incorporating wavelet filters into the CBJTC. The experimental results show that, firstly the noise suppression can be obtained by choosing appropriated compression level such that the stronger the noise, the smaller the compression level. Secondly, the retinal recognition obtained by incorporating the wavelet filters can be improved regardless of the noise level, yielding better recognition performance than the conventional Joint Transform Correlator (JTC) for the whole compression quality Quality Factor (QF).

School of Physics Student's Signature _____

Academic Year 2014 Advisor's Signature _____

ACKNOWLEDGEMENTS

The author would like to express his deep gratitude to his advisor, Prof. Dr. Joewono Widjaja for his invaluable guidance and inspiration during the course of his study in this department.

I would like to give special thanks to Prof. Dr. Yupeng Yan for providing scholarship. I would also like to thank Dr. Ubon Suripon for discussion of this thesis. I gratefully acknowledge Institute of Science, Suranaree University of Technology for granting a teaching assistantship and a thesis support.

Finally, I want to express my appreciation to my family, and all of my friends for their love and moral support.

Komin Kaewphaluk

CONTENTS

CONTENTS (Continued)

Page

CONTENTS (Continued)

Page

LIST OF FIGURES

Figure **Page**

LIST OF FIGURES (Continued)

Figure **Page**

LIST OF FIGURES (Continued)

Figure **Page**

LIST OF FIGURES (Continued)

Figure **Page**

LIST OF FIGURES (Continued)

Figure **Page**

LIST OF FIGURES (Continued)

Figure **Page**

LIST OF ABBREVIATIONS

CBJTC	Compression-Based Joint Transform Correlator
CBJWTC	Compression-Based Joint Wavelet Transform Correlator
CCD	Charge-Coupled Device
CR	Compression Ratio
DCT	Discrete Cosine Transform
EASLM	Electrically-Addressed Spatial Light Modulator
JPEG	Joint Photographic Experts Group
JPS	Joint Power Spectrum
JTC	Joint Transform Correlator
JWTC	Joint Wavelet Transform Correlator
PCD	Peak to Correlation Deviation
PSNR	Peak Signal-to-Noise Ratio
QF	Quality Factor
SD	Standard Deviation
WT	Wavelet Transform
WTC	Wavelet Transform Correlator

CHAPTER I

INTRODUCTION

1.1 Introduction

In the field of information optics, correlation-based pattern recognition has been widely implemented by using joint transform correlator (JTC). The reason for this interest is that the JTC can be implemented in the real time, because it does not require a prior synthesis of matched spatial filters (Jutamulia, 2003; Alsamman and Alam, 2003; Widjaja, 2007). In the optical implementation of the real-time JTC (Yu, Jutamulia, Lin and Gregory, 1987) a target image detected by a charge-coupled device (CCD) camera and a reference image stored in a computer system are displayed side-by-side onto an electrically-addressed spatial light modulator (EASLM) placed in a front focal plane of a Fourier transforming lens. By illuminating the EASLM perpendicularly with a coherent collimated beam, the displayed joint input images are optically Fourier transformed by the lens. As a result, the joint power spectrum (JPS) generated at the back focal plane of the lens is recorded by a CCD sensor. Finally, a correlation output is generated by redisplaying the recorded JPS onto the same EALM in order to be optically Fourier transformed.

However, the JTC performance has several limitations such as firstly, the time delay caused by a serial process of displaying the target and the reference images onto the EASLM is determined by file size of the images. Secondly, the JTC is sensitive to an inherent rotation and scale variances of the target. Therefore, a database of

the reference images must contain all possible variations of the rotation and the scale changes of the target.

In order to solves these problems, the reference images is compressed by using digital image compression such as that developed by the Joint Photographic Experts Group (JPEG) (Widjaja and Suripon, 2004). Therefore an implementation of the real-time JTC by using the compressed reference images can reduce the time delay in transferring the image from the computer system to the EASLM and the stringent storage requirement for storing the database.

To verify feasibility of the proposed method, biometric recognition by using human face and fingerprint images with different contrast and noise as test scenes has been studied (Pennebaker and Mitchell, 1993; Widjaja and Suripon, 2005; Widjaja and Suripon, 2006). The results show that although the compressed human face reference has small file size, the recognition using the proposed JTC gives better performance than that for the fingerprint recognition such that dependencies on contrast difference, noise level and compression quality are not significant. This is because the human face image contains less high-spatial-frequency components than the fingerprint does. When the human face image is used as the reference, an impulse response of the JTC becomes broader than the use of the high-contrast fingerprint as the reference. Consequently, degradation of the broad correlation signal caused by the contrast difference, noise and compression is less significant compared to that of the narrow correlation signal. Therefore, the proposed compression-based JTC (CBJTC) is suitable for recognition of biometrics having low spatial-frequency components such as retina images.

Furthermore, retina image is one of the most reliable and stable for identity authentication (Hill, Jain, Bolle and Pankanti, 1999; Jain, Ross and Prabhakar, 2004). This is because retina is rich in unique blood vessels and it is located at the back of eyes. Therefore, it is impossible to counterfeit retina images without cooperation from subjects or without using special recording instruments such fundus cameras which employs a high resolution image sensor. Since characteristics of human face and retina images are different, it is important to study feasibility of the retina recognition by using our proposed method.

1.2 Significance of Study

In this thesis work, retina recognition by using the JTC with compressed target and reference images is experimentally studied. The advantages of this work are that first by compressing both images, the image transfer time of the JTC can be further improved. Second, the compression of the noisy target can reduce noise (Al-Shaykh and Mersereau, 1998). Thus, the recognition performance can be further improved. Third, the proposed method can be applied to development of tele-ophthalmology (Basu et al., 2003; Conrath et al., 2007) where compressed retina images taken in remote areas are transmitted through telecommunication network to a regional center for screening by medical specialists. For these reasons, our proposed method can be used for both security recognition and initial screening of development of eye threatening diseases via a comparison of the recorded retina images taken at different time period (Kertes and Johnson, 2007). The present work focuses on experimental verifications of the retina recognition. The work takes into account a presence of an additive noise in the input target caused by an imperfect image acquisition system.

Although the conventional JTC can be employed to implement real-time pattern recognition, it has broad of correlation width and contains a strong zeroth-order term of the correlation output. In order to improve the retina recognition performance, a compression-based joint wavelet-transform correlator (CBJWTC) is proposed by incorporating wavelet filters into the CBJTC (Widjaja, 2010).

1.3 Research Objectives

1.3.1 To study experimentally the retina recognition by using the CBJTC.

1.3.2 To study effects of the JPEG compression of the retina target and reference images on the retina recognition in situation that the target is corrupted by additive Gaussian white noise.

1.3.3 To improve the retina recognition performance of the CBJTC by incorporating wavelet filters.

1.4 Scope and Limitation of the Study

This thesis studies experimentally the retina recognition by using the JTC with JPEG-compressed target and reference images. The recognition performance is studied by using high-contrast retina images with different noise level. The scope and limitations of the study are defined as follows.

- **Image compression scheme**

The ACD See software will be used to compress the reference and the target images into the JPEG format with various compression qualities. The quality is determined by QF whose value can be varied form 0-100. The higher the QF, the better the quality of the compress image will be. The reason for using the JPEG is that

it is one of the digital image compression standards and its format is widely supported by CCD sensors.

- **Retina image**

Original retina images are recorded by using a non mydriatic autofocus fundus camera (Nidek AFC-210). To have better contrast, a green channel of captured image is converted into 8-bit gray scale image. An area of 124 × 168 pixels around an optic disc is selected and use as test scene with file size of 101 Kbytes.

- **Measure of correlation output**

The correlation output is quantitatively measured by using a ratio of the correlation peak intensity to the standard deviation (SD) of the correlation intensity (PCD).

- **Retina recognition procedure**

In order to study experimentally the recognition performance of the CBJTC, a research procedure shown in Fig. 1.1 is implemented. The retina images are captured by using a non mydriatic autofocus fundus camera and duplicated into the target and the reference images. The Gaussian noises generated by using the IMNOISE command of MATLAB program are added to the retina targets. The retina target and the reference images are compressed into the JPEG format by using the ACDsee software with different compression levels. The retina recognition by using the CBJTC and the CBJWTC are then experimentally verified by using 2-*f* optical set up. The correlation outputs are quantitatively measured by using the PCD.

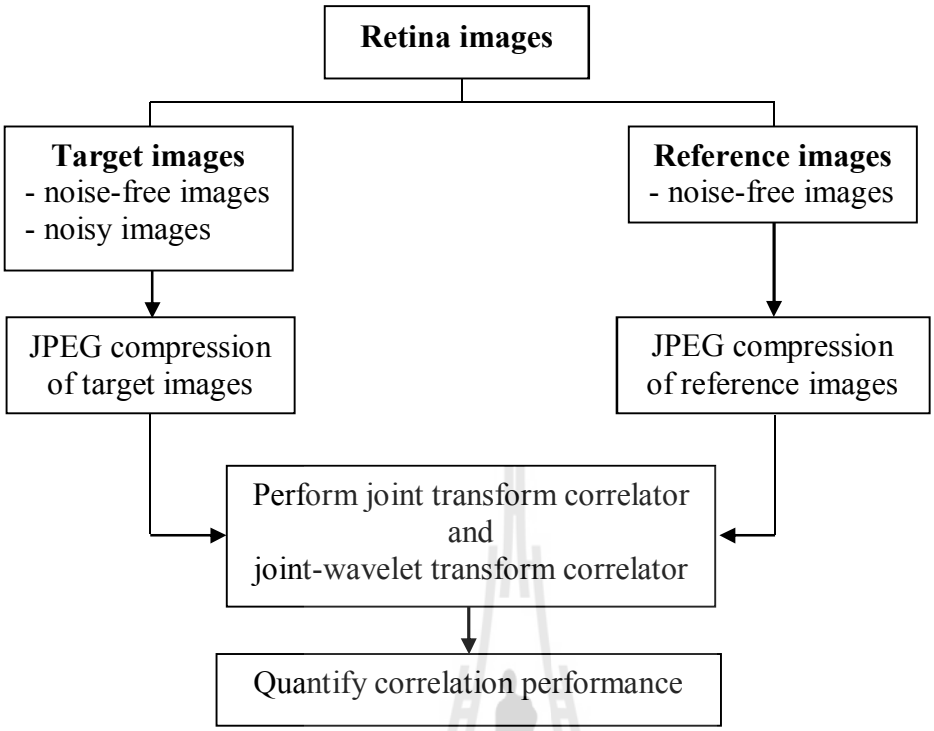

Figure 1.1 Diagram of the retina recognition by using the CBJTC and the CBJWTC.

1.5 Organization

This thesis consists of six chapters of which this is the first chapter. Chapter II reviews the concept of optical pattern recognition by using the JTC. The review starts with the principles of optical Fourier transform and is continued by discussing the classical JTC and the joint wavelet transform correlator (JWTC). In Chap. III, JPEG algorithm and an objective measure of image quality are presented. Chapter IV discusses the experimental verifications of the noisy retina recognition by using the CBJTC. Chapter V presents the improvement of the retina recognition by using the JWTC. Finally, the conclusions of the thesis are presented in Chapter VI.

CHAPTER II

OPTICAL PATTERN RECOGNITION BY USING JOINT TRANSFORM CORRELATOR

In this chapter, we review the concept of optical pattern recognition by using the JTC. The optical implementation of the joint transform correlator by using the Fourier transforming properties of a spherical lens is firstly reviewed. The implementation of the JTC by using wavelet filter is then discussed.

2.1 Introduction

A correlation operation measures a similarity of two input functions. In its implementation, a correlation of two functions that are the target and the reference images, can be obtained by taking an inverse Fourier transform of a product of the Fourier spectra of the two images. A height and sharpness of the correlation output give a degree of similarity between the two images.

In the field of information optics, correlation-based pattern recognition has been widely implemented by using coherent optical processing. A matched spatial filter is the first optical architecture proposed by Vander Lugt to perform image correlations (Lugt, 1964). However, the Vander Lugt correlator has drawbacks in that firstly it requires a prior fabrication of the matched spatial filters used in the correlation process. Note that the matched spatial filters are fabricated by recording an interference of a Fourier spectrum of the reference image and a plane reference

wave. Secondly, it requires a stringent alignment of the fabricated filters. On the other hand, the joint transform correlator does not require the interferometric fabrication of the matched spatial filters (Goodman, 1996) when it is implemented in conjunction with an EASLM, the joint transform correlator can be used for real-time pattern recognition.

2.2 Optical Fourier Transform

The optical implementation of the Fourier transform is based on the scalar diffraction theory and wave propagation of coherent light. The optical Fourier of a spatial mask with an amplitude transmittance $g(x,y)$ can be done by using a positive lens shown in Figure 2.1. By illuminating perpendicularly the mask placed at one focal length f in front of the lens with a coherent plane wave, the amplitude distribution generated at one focal length behind the lens can be mathematically expressed as (Goodman, 1996)

$$G(u,v)=\frac{1}{j\lambda f}\int_{-\infty}^{\infty}\int_{-\infty}^{\infty}g(x,y)\exp\left\{-j\frac{2\pi}{\lambda f}(xu+yv)\right\}dxdy, \tag{2.1}$$

where λ is the wavelength of the coherent light and (u,v) are the coordinates in the horizontal and the vertical directions at the back focal plane known as the Fourier plane.

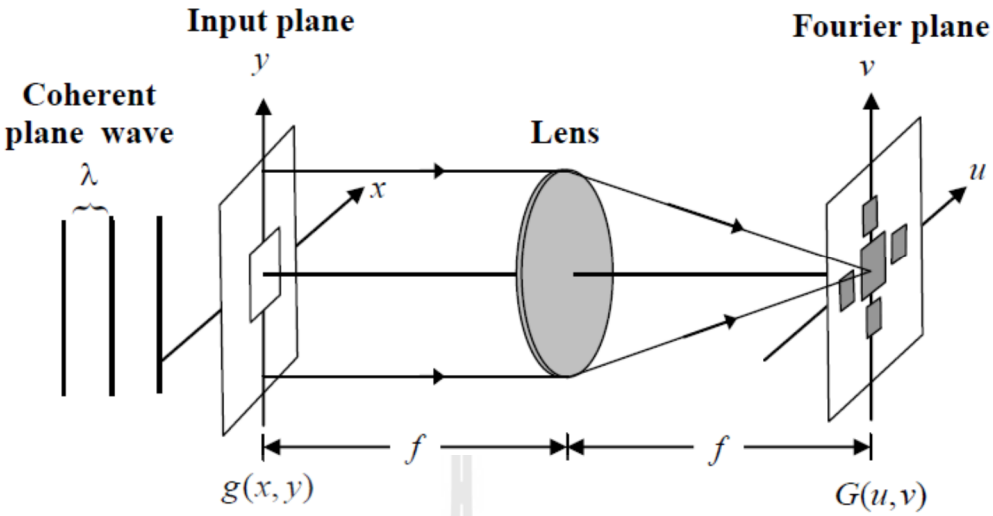

Figure 2.1 A schematic diagram of an optical setup for implementing the Fourier transform of the spatial mask $g(x,y)$ by using a positive lens (Widjaja, 2006).

2.3 Joint Transform Correlator

A basic operation of the joint transform correlator consists of a two-step process. The first step is the generation of the JPS of the target and the reference images by using the optical Fourier transform shown in Figure 2.2 (a). The target $t(x,y)$ and the reference $r(x,y)$ images are placed side-by-side on the input plane (x,y). This joint input image can be mathematically expressed as

$$f(x,y) = r(x - x_0, y) + t(x + x_0, y), \tag{2.2}$$

where x_0 and $-x_0$ are the position of the reference and the target images in the x direction at the input plane. By illuminating the joint input image with a coherent

collimated beam, the Fourier spectrum of the joint input image is generated at the Fourier plane as

$$F(u,v)=\frac{1}{j\lambda f}\left[R\ (u,v)\exp\left(-j\frac{2\pi x_0 u}{\lambda f}\right)+T\ (u,v)\exp\left(j\frac{2\pi x_0 u}{\lambda f}\right)\right], \qquad (2.3)$$

where $R(u,v)$ and $T(u,v)$ are the Fourier transforms of the reference and the target images, respectively.

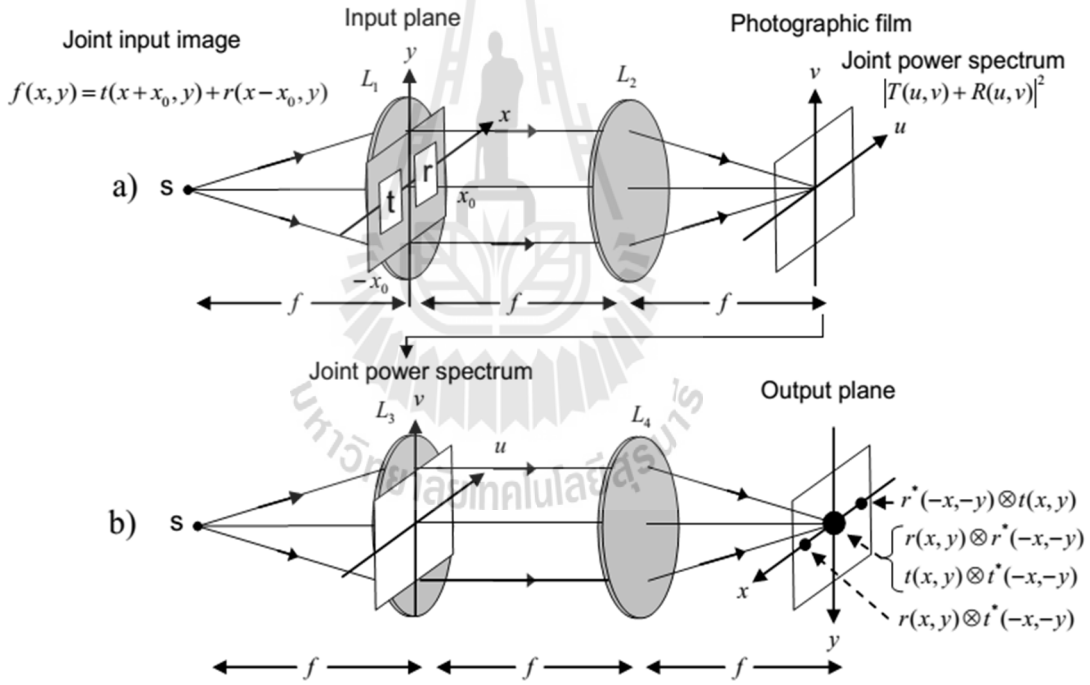

Figure 2.2 A schematic diagram of an optical setup for implementing the joint transform correlator. (a) A generation of the joint power spectrum and (b) a generation of the correlation output (Goodman, 1996).

In Eq. (2.3), the exponential terms are caused by the spatial translation of the joint input image at the input plane. The intensity of this complex field distribution recorded on a photographic film or light-sensitive recording medium can be mathematically expressed as

$$\begin{aligned} I(u,v) &= |F(u,v)|^2 \\ &= \frac{1}{\lambda^2 f^2}\left| R(u,v)\exp\left(-j\frac{2\pi x_0 u}{\lambda f}\right) + T(u,v)\exp\left(j\frac{2\pi x_0 u}{\lambda f}\right)\right|^2 \\ &= \frac{1}{\lambda^2 f^2}\left[|R(u,v)|^2 + |T(u,v)|^2 + R(u,v)T^*(u,v)\exp\left(-j\frac{4\pi x_0 u}{\lambda f}\right)\right. \\ &\qquad \left. + T(u,v)R^*(u,v)\exp\left(j\frac{4\pi x_0 u}{\lambda f}\right)\right]. \end{aligned} \tag{2.4}$$

In Eq. (2.4), the last two terms are associated to the multiplications of the Fourier spectra of the reference and target images.

In the second step, the recorded joint power spectrum is Fourier transformed in order to generate the correlation output. This is done by placing the recorded power spectrum in the input plane of the optical setup shown in Figure 2.2 (b). The Fourier transform by the lens L_4 gives the correlation output

$$\begin{aligned} g(x,y) = \frac{1}{\lambda f}\big[& r(x,y)\otimes r^*(-x,-y) + t(x,y)\otimes t^*(-x,-y) \\ & + r(x,y)\otimes t^*(-x,-y)\otimes\delta(x-2x_0) \\ & + t(x,y)\otimes r^*(-x,-y)\otimes\delta(x+2x_0)\big], \end{aligned} \tag{2.5}$$

where $\otimes$ denotes the convolution operation and $*$ is the complex conjugate. The first two terms in Eq. (2.5) give the zeroth-order peak appeared at the origin. They correspond to the sum of the autocorrelations of the reference and the target images.

The last two terms are the desired cross-correlations of the input target and the reference images which appear at the positions $+2x_0$ and $-2x_0$ on the correlation plane, respectively.

The position of the correlation terms in Eq. (2.5) is shown in Figure 2.3. The cross-correlation terms are separated from the zeroth order terms by $2x_0$. If W_t and W_r represent the maximum width in the x direction of the target and the reference, respectively, the zeroth-order component occupies an area between $-\max\{W_t, W_r\}$ and $\max\{W_t, W_r\}$. Whereas, the cross-correlation components extend from $\pm[2x_0 - (W_t + W_r)/2]$ to $\pm[2x_0 + (W_t + W_r)/2]$. Therefore, in order to separate the desired terms from the zeroth-order term, the following conditions must be satisfied

$$2x_0 - \frac{W_t + W_r}{2} > \max\{W_t + W_r\}$$

or

$$2x_0 > \max\{W_t + W_r\} + \frac{W_t + W_r}{2}. \tag{2.6}$$

Finally, by measuring the height and the sharpness of the desired cross-correlation output, the degree of similarity between the target and the reference can be finally determined.

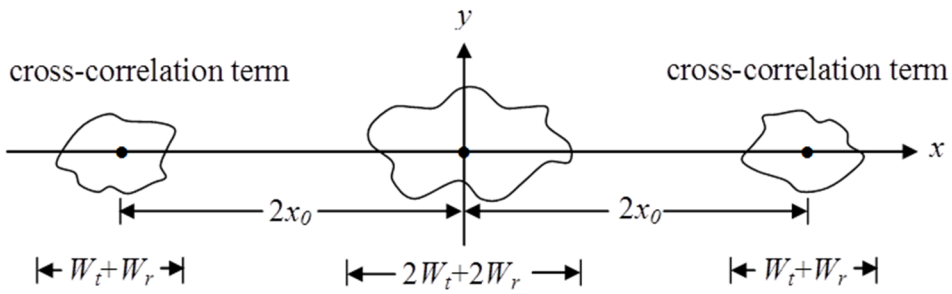

Figure 2.3 Locations of the correlation terms at the correlation plane (Widjaja, 2006).

2.4 Wavelet Transform

Wavelet transform (WT) is one of the most popular techniques in images processing. It has been widely applied into many real-world problems of pattern recognition, images compression and signal detection, because the WT can be used to analyze non-stationary signals in space and frequency domain. The WT of a 2-D signal $f(x,y)$ (Allen and Rabiner, 1977) is defined as

$$W_f(a_x,a_y,b_x,b_y)=\int_{-\infty}^{\infty}\int_{-\infty}^{\infty} f(x,y)h^*_{a_xa_yb_xb_y}(x,y)dxdy, \tag{2.7}$$

where $h^*_{a_xa_yb_xb_y}(x,y)$ is the complex conjugate of the daughter wavelet $h_{a_xa_yb_xb_y}(x,y)$ generated by dilation (a_x,a_y) and translation (b_x,b_y) of the mother wavelet $h(x,y)$. A daughter wavelet (Roberge and Sheng, 1994) is defined as

$$h_{a_xa_yb_xb_y}(x,y)=\frac{1}{\sqrt{a_xa_y}}h\left(\frac{x-b_x}{a_x},\frac{y-b_y}{a_y}\right). \tag{2.8}$$

The mother wavelet $h(x,y)$ must satisfy the admissible condition (Young, 1993) such as

$$\left|H(u,v)\right|^2 = 0 \text{ for } u = v = 0, \tag{2.9}$$

and

$$\int_{-\infty}^{\infty} h(x,y)dxdy = 0. \tag{2.10}$$

This condition shows that the mean of the mother wavelet must equal to zero or its spectrum $H(u,v)$ has a zero dc component. The corresponding Fourier transform of the daughter wavelet $H_{a,b}(u,v)$ (Marr and Hildreth, 1980) is given by

$$H_{a,b}(u,v) = \mathcal{F}\left\{h_{a,b}(x,y)\right\} = \sqrt{a_x a_y}\, H(a_x u, a_y v)\exp[-i2\pi(b_x u + b_y v)]. \tag{2.11}$$

In the Fourier domain, the WT defined by Eq. (2.7) becomes

$$W_f(a_x, a_y, b_x, b_y) = \sqrt{a_x a_y}\int_{-\infty}^{\infty}\int_{-\infty}^{\infty} F(u,v)H^*(a_x u, a_y v)\exp[i2\pi(ub_x + vb_y)]dudv, \tag{2.12}$$

where $F(u,v)$ and $H(a_x u, a_y v)$ are the Fourier transform of the signal $f(x,y)$ and the daughter wavelet $h_{a_x a_y b_x b_y}(x,y)$, respectively.

One of the useful wavelet functions is the Mexican-hat wavelet which is a second derivative of a Gaussian function. The 2D Mexican-hat wavelet is given by

$$h(x,y) = \frac{1}{\sigma^3\sqrt{2\pi}}\left(\frac{x^2}{\sigma^2} + \frac{y^2}{\sigma^2} - 1\right)\exp\left(-\frac{x^2+y^2}{2\sigma^2}\right), \tag{2.13}$$

where the Gaussian function has the form of

$$G(x,y) = \frac{1}{\sigma\sqrt{2\pi}}\exp\left(-\frac{x^2+y^2}{2\sigma^2}\right) \tag{2.14}$$

with σ is the standard deviation of the distribution. The plots of the Mexican-hat function and its Fourier transform are shown in Figures 2.4 (a) and (b), respectively. In Figure 2.4 (a), the Mexican-hat function has a high peak at the origin and two negative lobes located on the other sides of that peak. The mean value of this function is zero, while its spectrum shown in Figure 2.4 (b) has zero dc component. This means that the Mexican-hat wavelet function can localize frequency information of the signal being analyzed.

Figure 2.5 shows the Fourier spectrum of the Mexican-hat wavelet $H_a(u,v)$ as function of the dilation factor. When the mother wavelet is dilated by a small factor a, the wavelet filter is expanded which results in a high center frequency and wide bandwidth.

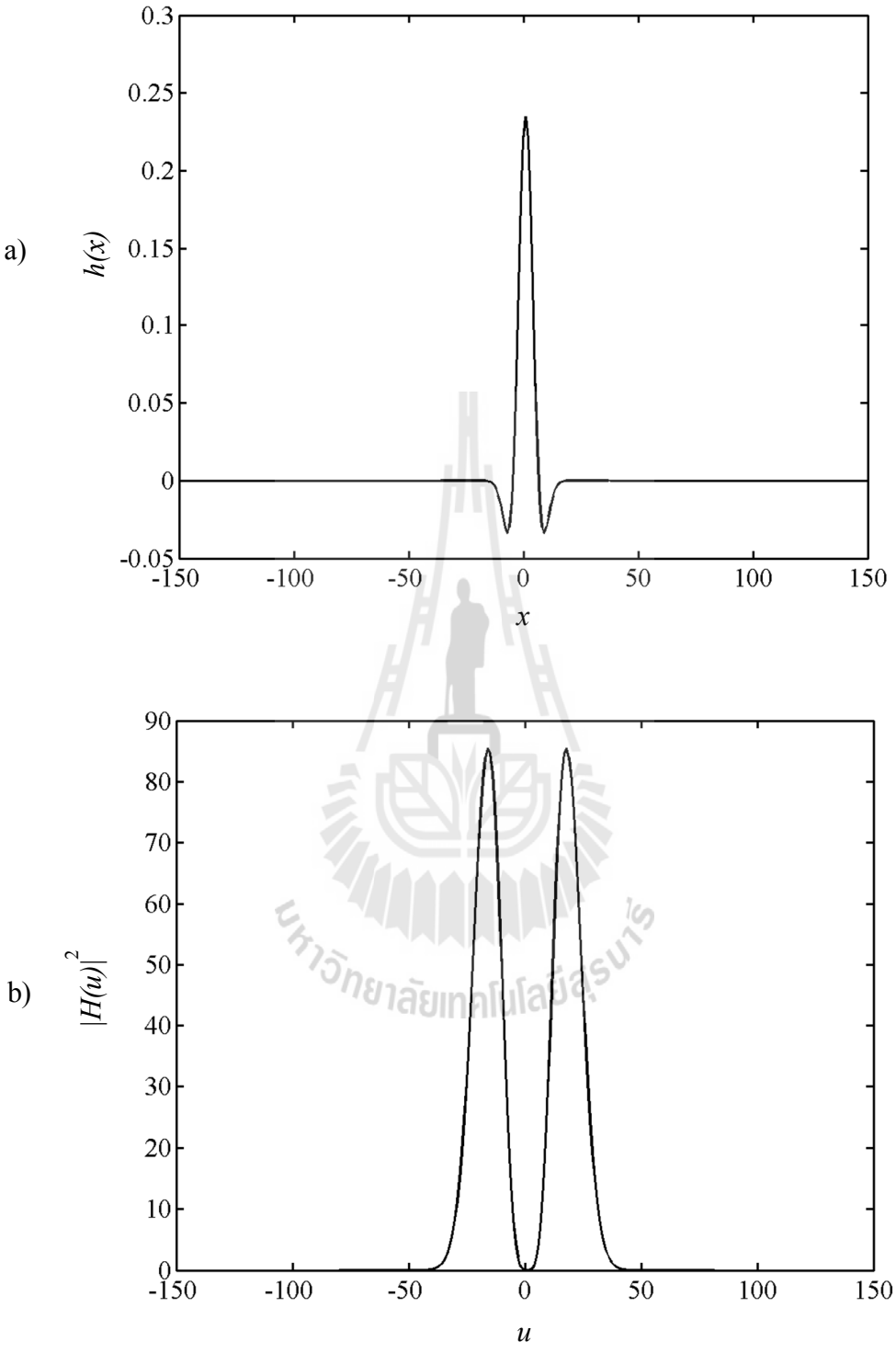

Figure 2.4 (a) The Mexican-hat mother wavelet and (b) its power spectrum.

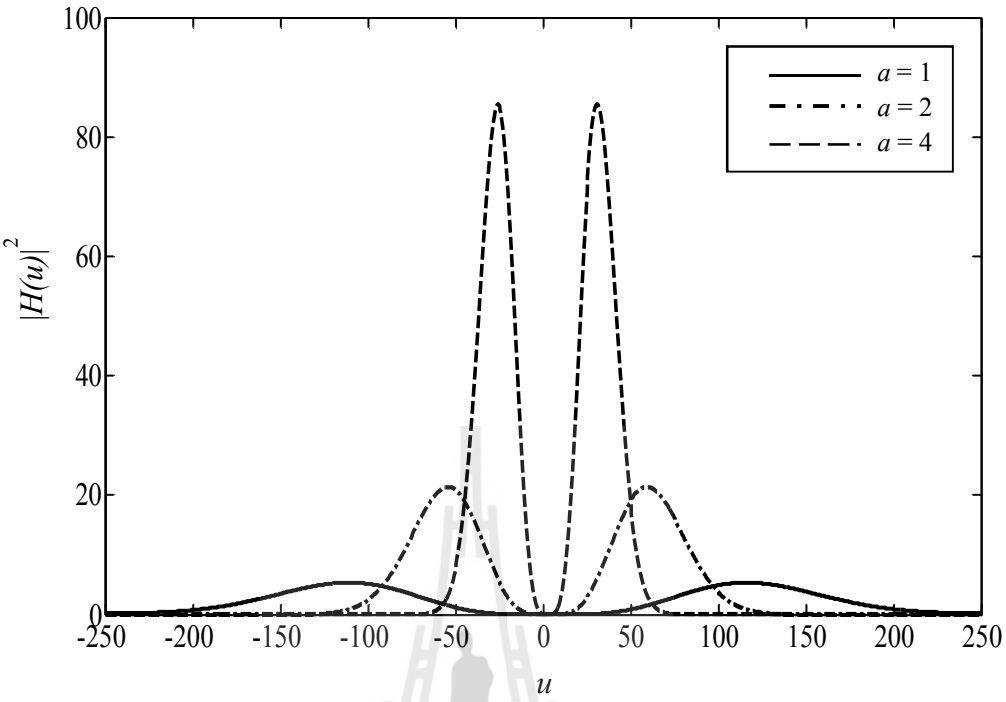

Figure 2.5 Power spectra of the Mexican-hat wavelet for different dilation factors.

When a is large, the wavelet filter is compressed with low center frequency and narrow bandwidth. In the WT concept, the wavelet function corresponds to a band-pass filter which operates at constant relative the bandwidth so-called constant-Q factor

$$Q = \frac{u_0}{\Delta u}. \tag{2.17}$$

Here, u_0 is the center frequency and Δu denotes the bandwidth. If the spatial width and the bandwidth of the wavelet function are regarded as the spatial and the frequency resolutions, respectively. The small dilation factor corresponds to the wavelet analysis with high spatial resolution and low frequency resolution. Whereas

the large dilation factor gives a wavelet analysis with low spatial resolution and high frequency resolution. This property is known as the multi-resolution of the WT.

2.5 Wavelet Transform Correlator

Wavelet transform correlator (WTC) can be used to improve recognition performance of the conventional JTC. This is because the multi-resolution property of the WT can detect multi-scale edge features of signals (Mallat and Hwang, 1992; Mallat and Zhong, 1992). Since edges provide boundaries which are significant images features, the edge enhancement by using the WT can be useful for the pattern recognition.

The WTC is the correlation between the WT of the target signal and the reference signal (Sheng, Roberge, Szu and Lu, 1993).

$$c(a_x, a_y, x, y) = \int_{-\infty}^{\infty}\int_{-\infty}^{\infty} W_f(a_x, a_y, b_x, b_y) W_r^*(a_x, a_y, b_x - x, b_y - y) db_x db_y, \qquad (2.18)$$

where $W_f(x, y)$ and $W_r(x, y)$ are the wavelet transforms of the target $f(x, y)$ and reference image $r(x, y)$, respectively. The WTC in the Fourier domain (Widjaja, 2003) can be calculated as

$$c(a_x, a_y, x, y) = \int_{-\infty}^{\infty}\int_{-\infty}^{\infty} F(u, v) R^*(u, v) \left| H(a_x u, a_y v) \right|^2 \exp[-i2\pi(xu + yv)] du dv, \qquad (2.19)$$

where $F(u,v)$, $R(u,v)$, and $H(a_x u, a_y v)$ associate with the Fourier transforms of the target $f(x,y)$, the reference $r(x,y)$, and the daughter wavelet function $h_{a_x a_y b_x b_y}(x,y)$, respectively.

CHAPTER III

JPEG IMAGE COMPRESSION

JPEG is an acronym for joint photographic experts group which is a compression algorithm widely employed by image sensors. The JPEG algorithm gives a higher compression level than a lossless compression algorithm. In this chapter, the algorithm of the JPEG compression is reviewed in Sect. 3.1. In image compressions, quality of the compressed image is measured by a parameter called the quality factor (QF). The higher the QF implies the better the quality of the compress image. In Sect. 3.2, the JPEG compression of retina images is discussed. Finally, the measures of image quality are presented in Sect. 3.3.

3.1 JPEG Compression Scheme

The JPEG algorithm is one of the most widely used image compression standards which is designed for either full-color or gray scale digital images. This algorithm exploits a limitation of the human eye in perceiving small color and intensity variations. The basis of the JPEG algorithm is to remove high spatial frequency components by means of a discrete cosine transform (DCT) (Pennebaker and Mitchell, 1993). Figure 3.1 shows a block diagram for implementing the JPEG algorithm. First, picture elements of the image to be compressed is divided into blocks of 8×8 pixels. Second, the DCT is applied to each block to produce its spatial frequency components The transform generates 1 DC and 63 AC components of

spatial frequency. The DC frequency component represents the average value in the block, while the AC terms represent intensity changes within the block. As the high- and low-frequency components are separated out, the high-frequency components are easily removed without affecting the low-frequency information. Third, each of the 64 DCT components is quantized in conjunction with a quantization table. This is done in such a way that high spatial-frequency components are quantized with higher quantization coefficients than the lower spatial-frequency ones. After the quantization, the results are rounded to integers. This causes irretrievable loss of information. As a consequence, the AC components almost vanish. Fourth, the 64 quantized frequency components are encoded by using a combination of run-length encoding and Huffman coding.

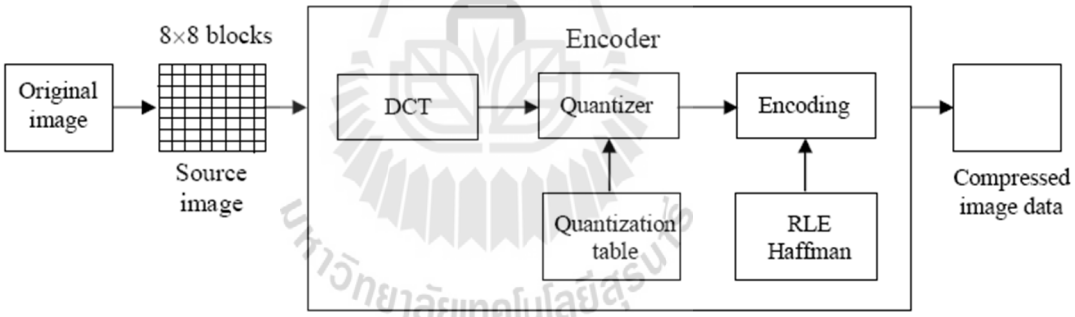

Figure 3.1 A block diagram of the JPEG encoder (Salomon, 1998).

3.2 JPEG Compression of Retina Images

In order to study the effect compression on the recognition performance of the joint transform correlator, the original retina image shown in Figure 3.2 (a) was recorded by using a non mydriatic autofocus fundus camera (Nidek AFC-210). To get a better contrast, a green channel of the captured image was converted into an 8-bit gray scale image. An input image around an optic disc with an area of 124 × 168

pixels was used as the test scene with file size of 101 Kbytes. This input image was duplicated as the target and the reference images shown in Figure 3.2 (b).

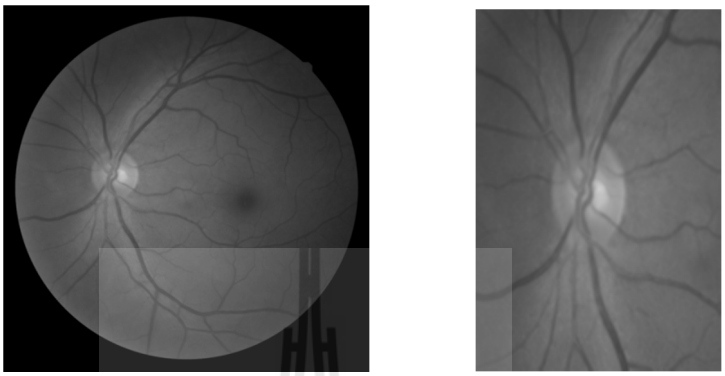

(a) (b)

Figure 3.2 The retina images. (a) The original and (b) the test images.

They were compressed into the JPEG format by using the ACDSee Photo Manager version 3.1 software (ACD systems, Ltd.) with various compression qualities. In this software, the QF of the compressed images is varied from 0 to 100. A

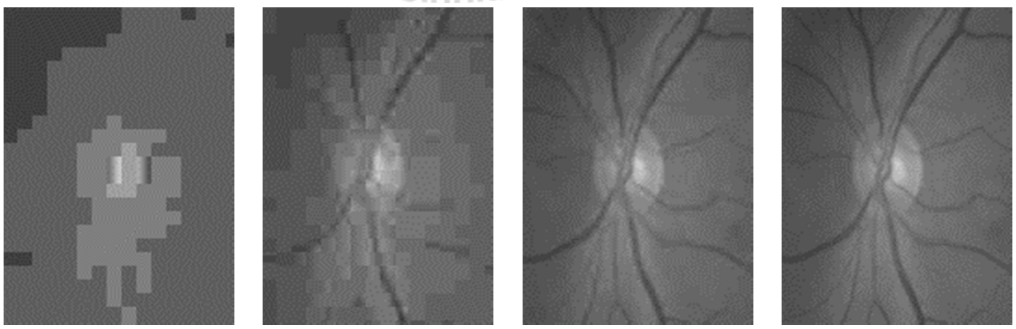

(a) (b) (c) (d)

Figure 3.3 Retina images compressed with the QF equals to (a) 0, (b) 10, (c) 40 and (d) 100.

large value of the QF discards less information than that of the small value. Thus, the higher the value of the QF, the better the image quality and the bigger the file size of the compressed image. Figure 3.3 shows the retina images compressed with the QF= 0, 10, 40 and 100. The regular pattern of visible block boundary which appears at the low QF is called the blocking artifacts (Pennebaker and Mitchell, 1993). Figure 3.4 shows the compression ratio (CR) defined as the file size ratio of the original to the JPEG compressed images as a function of the QF. It is clear that the CR becomes higher as the QF decreases, because the high compression ratio corresponds to the small file size of the compressed image.

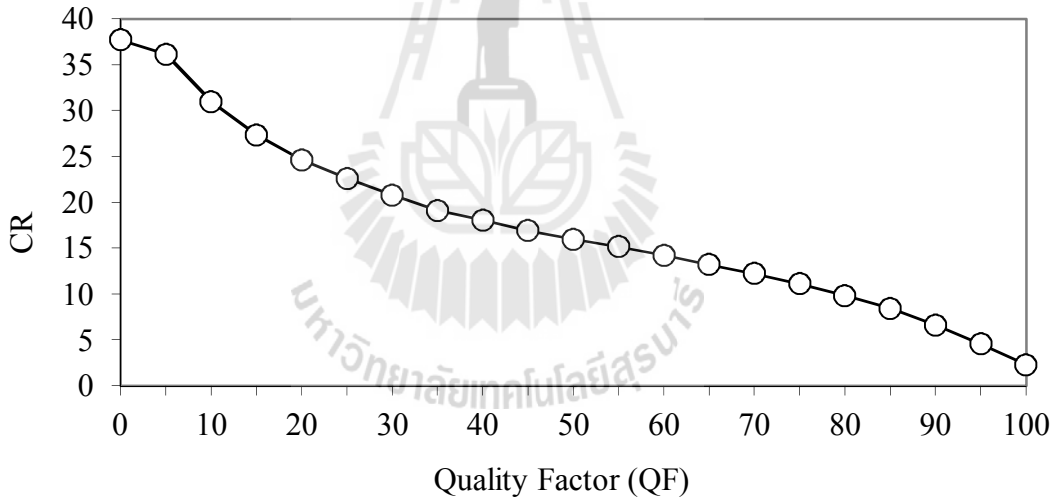

Figure 3.4 The compression ratio of the JPEG compressed high-contrast retina images as function of the QF.

3.3 Measures of Image Quality

In image processing, the peak signal-to-noise ratio (PSNR) is generally used for measuring the quality of the image compression. The PSNR is the ratio between the maximum possible pixels value and the mean-squared error of the differences in

the pixel values between the corresponding pixels of the two images (Yang, Zhang and Mitra, 1999)

$$PSNR = 10\log_{10}\left(\frac{255^2}{\frac{1}{M\times N}\sum_{i=0}^{M=1}\sum_{j=0}^{N=1}[f(i,j)-f_c(i,j)]^2}\right), \tag{3.1}$$

where $f(i,j)$ and $f_c(i,j)$ are the original and the compressed images with dimensions of $M \times N$ pixels, respectively. For 8 bits gray scale images, $f(x,y)$ has integer values between 0 and 255. Therefore, 255 is the maximum possible pixels value. This formula shows the degree of similarity between the original and the compressed images. A larger PSNR indicates that the degree of similarity between the original and the compressed images is higher or better the quality of the compressed images. Figure 3.5 shows the PSNR of the compressed retina images as a function of the compressed retina images as a function of QF. The PSNR becomes lower as the QF decreases. This is because as the QF becomes smaller, more information is discarded by the compression. Consequently, the degree of similarity decreases.

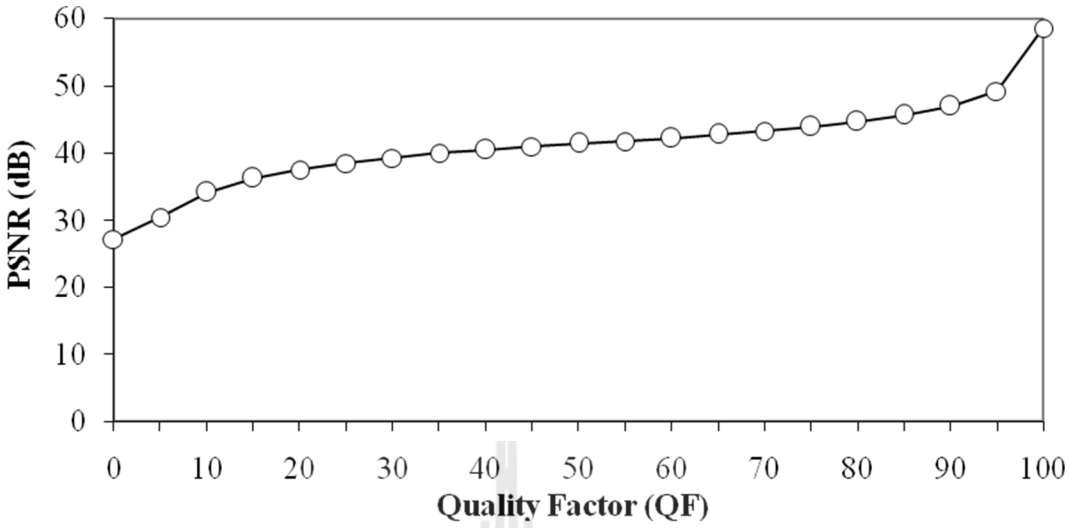

Figure 3.5 The compression ratio of the JPEG compressed high-contrast retina images as function of the QF.

CHAPTER IV

REAL-TIME JOINT TRANSFORM CORRELATOR USING COMPRESSED IMAGES

This chapter reports the experimental verifications of the retina recognition by using the joint transform correlator with the JPEG-compressed reference image (Widjaja and Kaewphaluk, 2014). The recognitions of the compressed noise-free and noisy targets are compared with the ones without compressions. The experimental results show that the recognition performance of the CBJTC can be improved by compressing the noisy targets. This is because loss of the high spatial-frequency components of the retina target does not only reduce the target file size but also the noise. In Sect. 4.1, the principle of the real-time JTC by using the compressed images is described. The experimental setup for implementing the real-time JTC with the compressed images is presented in Sect. 4.2. The last three sections discuss the experimental recognitions of the compressed noise-free and noisy targets.

4.1 Introduction

In the past decades, optical devices such as a magneto-optic device, a liquid crystal television, an EASLM and a CCD sensor have been used for real-time implementation of the JTC (Yu and Lu, 1984). The reason for this interest is that they can display the joint input image and record the JPS, replacing photographic films.

When the JTC is implemented by using the EASLM, a process of displaying the images from the computer system to the EASLM causes time delay which is dependent upon file size of the images. Besides this problem, considerable storage will be required for storing a database of the reference images. To solve these problems, the JPEG compression is applied to reduce file size of the retina images. Therefore, the implementation of the real-time JTC by using compressed retina images has advantages in that it reduces the recognition time and the storage requirement of the database.

A schematic diagram of the optical setup for implementing the real-time JTC by using compressed retina images is shown in Figure 4.1. The retina target image is captured by the CCD camera, while a set of reference images is stored in the computer system. In order to do the correlation, the joint image of the compressed target $t_C(x,y)$ and reference $r_C(x,y)$ are projected side-by-side onto the EASLM placed in the front focal plane of the Fourier transforming lens L_1. The joint compressed image (Widjaja and Suripon, 2011) can be expressed as

$$f(x,y) = r_C(x - x_0, y) + t_C(x + x_0, y) + n_C(x + x_0, y), \tag{4.1}$$

where $n_C(x,y)$ corresponds to the additive white Gaussian noise. Under illumination of a coherent collimated beam with a wavelength λ, the displayed images are optically Fourier transformed by the lens L_1. The joint Fourier spectrum $F(u,v)$ obtained at the Fourier plane can be expressed as

$$F(u,v) = R_C(u,v)\exp(-j2\pi x_0 u) + T_C(u,v)\exp(j2\pi x_0 u) + N_C(u,v)\exp(j2\pi x_0 u). \quad (4.2)$$

Here, $R_C(u,v)$, $T_C(u,v)$ and $N_C(u,v)$ are the Fourier spectra of the compressed reference $r_C(x,y)$, the compressed target $t_C(x,y)$ and the noise $n_C(x,y)$, respectively.

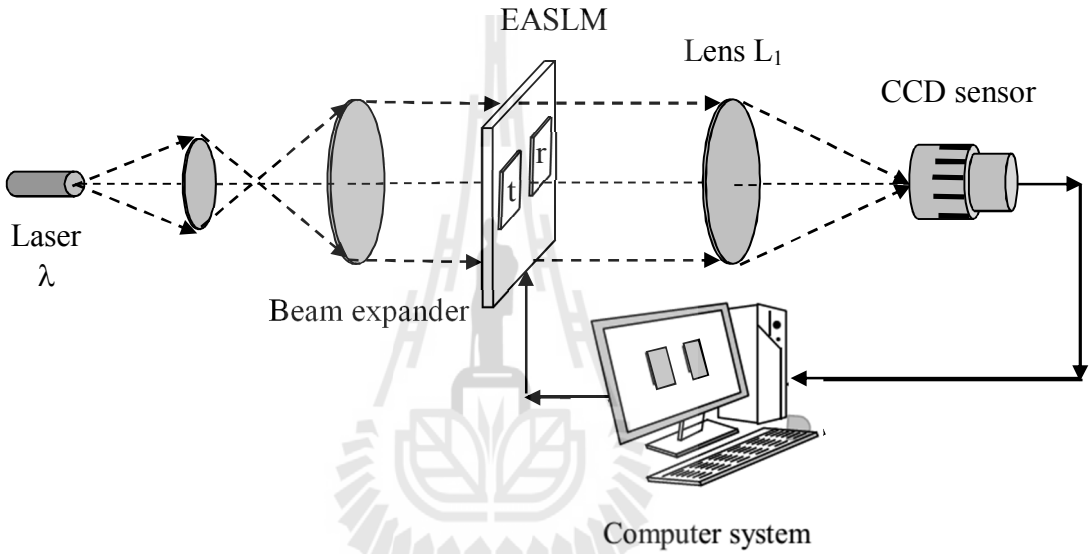

Figure 4.1 A schematic diagram of an optical setup for implementing the real-time JTC by using compressed retina images.

The intensity distribution of the joint power spectrum $I(u,v)$ recorded by a CCD sensor is mathematically equal to

$$
\begin{aligned}
I(u,v) &= \left|F\ (u,v)\right|^2 \\
&= \left|R_C(u,v)\exp(-j2\pi x_0 u) + T_C(u,v)\exp(j2\pi x_0 u) + N_C(u,v)\exp(j2\pi x_0 u)\right|^2 \\
&= \left|R_C(u,v)\right|^2 + \left|T_C(u,v)\right|^2 + \left|N(u,v)\right|^2 + T_C^*(u,v)N(u,v) + T_C(u,v)N_C^*(u,v) \\
&\quad + R_C(u,v)T_C^*(u,v)\exp(-j4\pi x_0 u) + T_C(u,v)R_C^*(u,v)\exp(j4\pi x_0 u) \\
&\quad + R_C(u,v)N_C^*(u,v)\exp(-j4\pi x_0 u) + N_C(u,v)R_C^*(u,v)\exp(j4\pi x_0 u). \qquad (4.3)
\end{aligned}
$$

In Eq. (4.3), the terms $R_C(u,v)T_C^*(u,v)$ and $T_C(u,v)R_C^*(u,v)$ are the products between the Fourier spectra of the compressed reference and target images. These terms produce the desired correlation. By redisplaying the recorded JPS onto the EASLM, the Fourier transformation by the lens L_1 gives the correlation output at the back focal plane as

$$
\begin{aligned}
g(x,y)\ \alpha\ \big[& r_C(x,y)\otimes r_C^*(-x,-y) + t_C(x,y)\otimes t_C^*(-x,-y) + n_C(x,y)\otimes n_C^*(-x,-y) \\
& + t_C^*(-x,-y)\otimes n_C(x,y) + t_C(-x,-y)\otimes n_C^*(x,y) \\
& + r_C(x,y)\otimes t_C^*(-x,-y)\otimes\delta(x-2x_0) \\
& + t_C(x,y)\otimes r_C^*(-x,-y)\otimes\delta(x+2x_0) \\
& + r_C(x,y)\otimes n_C^*(-x,-y)\otimes\delta(x-2x_0) \\
& + n_C(x,y)\otimes r_C^*(-x,-y) * \delta(x+2x_0)\big]. \qquad (4.4)
\end{aligned}
$$

The sixth, the seventh, the eighth and the ninth terms of Eq. (4.4) can be expressed as

$$
r_C(x,y) * t_C(x,y) * \delta(x \pm 2x_0) + r_C(x,y) * n_C(x,y) * \delta(x \pm 2x_0). \qquad (4.5)
$$

The first term of Eq. (4.5) is the desired correlation output of the compressed reference $r_C(x,y)$ and the compressed target $t_C(x,y)$. The second term is unwanted correlation output of the compressed reference $r_C(x,y)$ and the compressed noise $n_C(x,y)$. The both of correlation terms appear at the same positions $\pm 2x_0$ on the

correlation plane (x, y). It implies that besides the image qualities of the compressed reference and the compressed input target, the correlation output depends also on the compressed noise. Therefore, it is important to study the effects of image compression on the JTC.

4.2 Experimental Verifications

The experimental setup for implementing the real-time JTC by using the compressed reference and target images is depicted in Figure 4.2. The coherent light was generated from a He-Ne laser (Uniphase: 1507P-0) operating at a wavelength of 632.8 nm. A beam expander BE was constructed by combining a 20x microscope objective lens with focal length f = 8.3 mm, a 25 μm pinhole aperture used to clean up the spatial profile of the laser beam, and a positive lens with a focal length f = 300 mm. The resultant collimated beam had a diameter of about 36 mm. The beam was then used to illuminate the EASLM (Jenoptik SLM-M/460) with resolution of 832 × 624 pixels, pixel pitch of 32 μm × 32 μm and pixel size of 27 μm × 23 μm placed at the front focal plane of the Fourier transform lens L_1 with focal length f = 300 mm. The joint power spectrum at the back focal plane of the lens L_1 was detected by an eight-bit CCD sensor (PULNIX TM-2016-8) having pixel resolution of 1920 × 1080, pixel size and pitch of 7.4 μm × 7.4 μm. To reduce clipping of cosine fringes of the JPS from the high intensity of laser beam, a neutral density filter or ND filter with the optical density of about 2.2 was placed in front of the laser source. This is because the dynamic range of the sensor is limited.

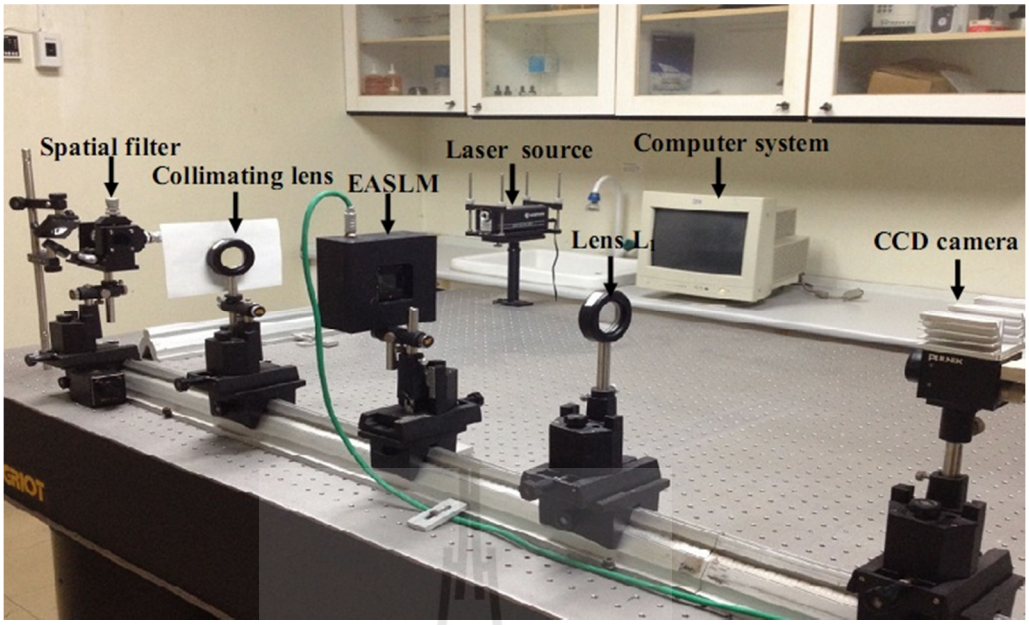

Figure 4.2 The experimental setup for implementing the real-time JTC with the compressed images.

The retina target without noise and corrupted by the noise with variance σ^2 = 0.01 and 1 are shown in Figure 4.3. They consisted of 124 × 186 pixels. All of the Gaussian noises were generated by using the IMNOISE command of the MATLAB software. In comparison with the noise-free images, it is clear that the degree of image degradation is the highest for the noise with variance $\sigma^2 = 1$.

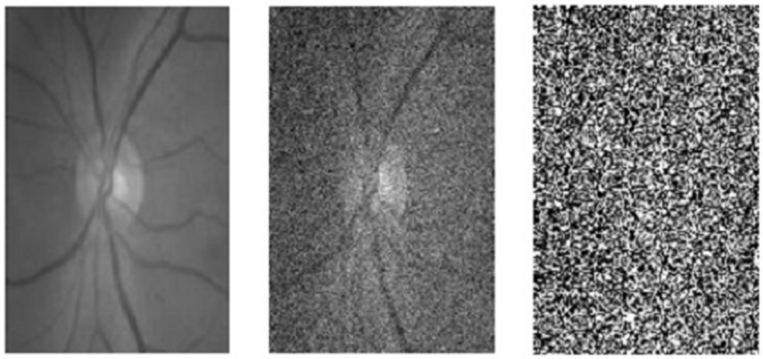

Figure 4.3 Retina images: (a) without noise and corrupted by (b) weak ($\sigma^2 = 0.01$) and (c) strong ($\sigma^2 = 1$) noises.

By displaying the target and the reference retina images side by side onto the EASLM, its JPS was captured by the CCD camera. The resultant JPS is shown in Figure 4.4. The fringe pattern caused by the interference between the target and reference beams can be obviously observed from the enlarged zeroth order of the JPS with the size 300 × 300 pixels shown in Figure 4.4 (b). The intensity of the zeroth order of the JPS is brighter than that of the higher order. Owing to the modulation of a broad sinc function, the zeroth-order of the JPS has the highest intensity, while the higher orders are attenuated.

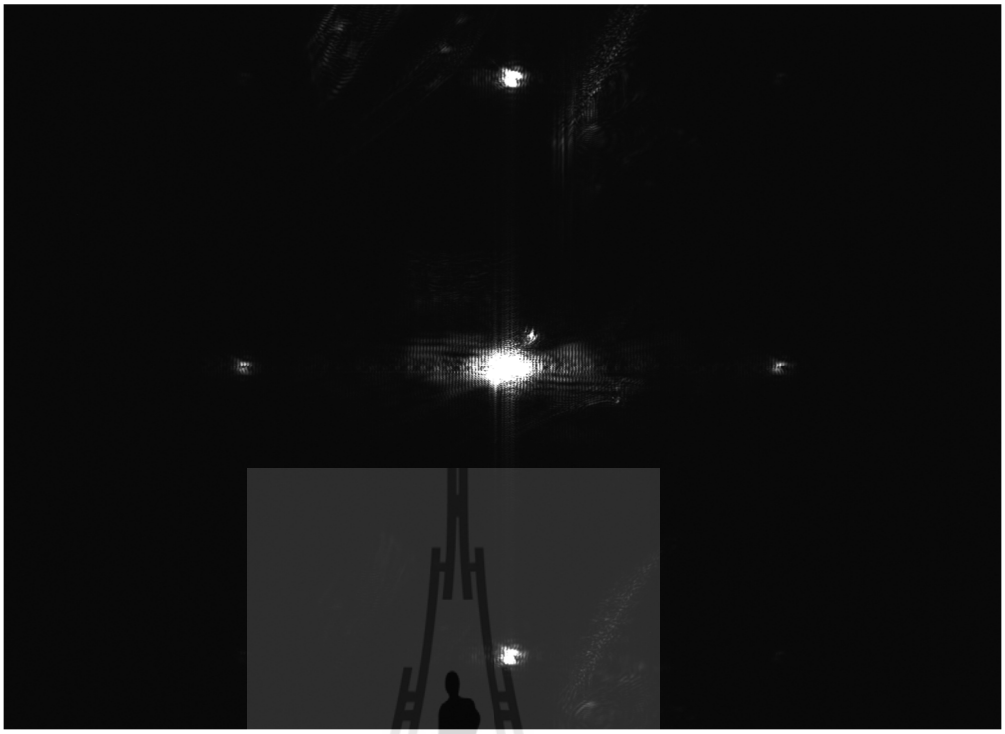

(a)

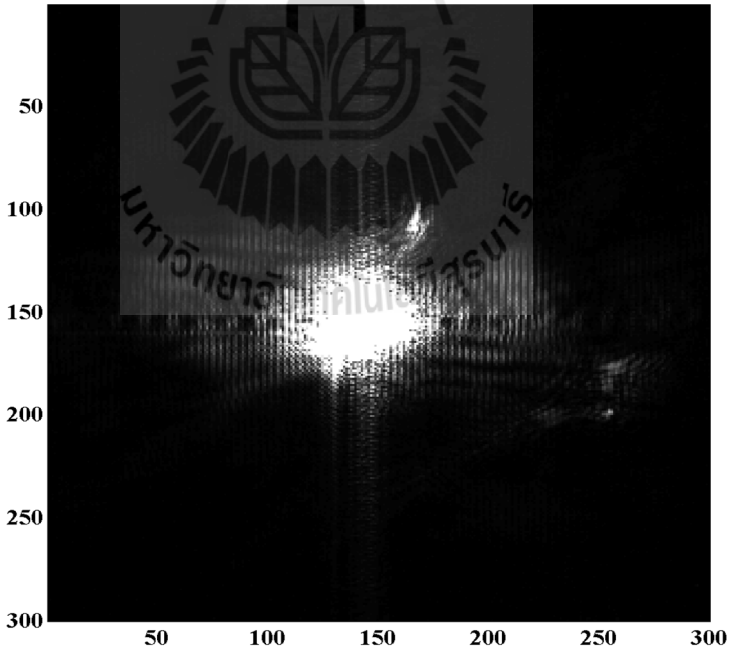

(b)

Figure 4.4 (a) The zeroth-order of the JPS of two identical noise-free retina images and (b) its enlarged zeroth order of the JPS.

The correlation output was generated by redisplaying the zeroth order of the JPS shown in Figure 4.4 (b) on to the EASLM. Figure 4.5 shows the correlation output of the identical uncompressed retina images generated by the setup shown in Figure 4.2.

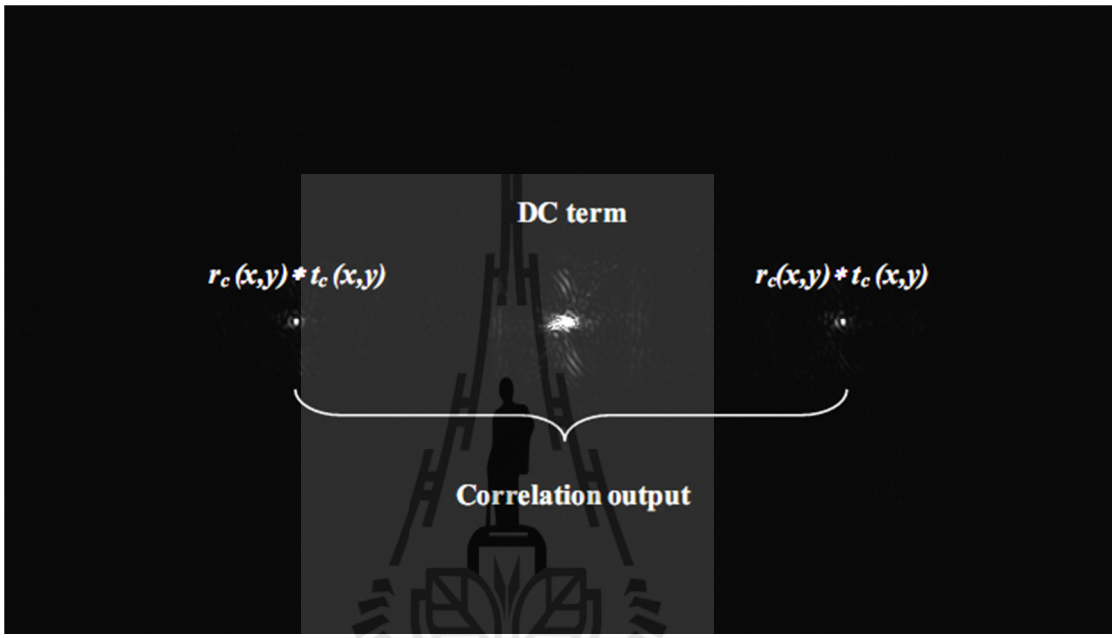

Figure 4.5 Autocorrelation output of the uncompressed retina image.

There are three bright spots along the horizontal direction. The center spot is the brightest than the other spots. According to Eq. (2.5), it corresponds to the first two terms of the JTC output which are the autocorrelation of the compressed target and that of the compressed reference. The other two spots represent the cross correlation outputs of the target and the reference images which are separated from the center spot by $2x_0$. The correlation quality of the JTC output is quantified by measuring the ratio of the correlation peak intensity to the standard deviation (SD) of the correlation intensity (PCD) (Roberge and Sheng, 1994) given by

$$PCD = \frac{I(i,j)_{\max}}{\left\{\frac{1}{M \times N}\sum_{i=0}^{M-1}\sum_{j=0}^{N-1}\left[I(i,j) - E\{I(i,j)\}\right]^2\right\}^{1/2}}. \quad (4.6)$$

Here, $I(i,j)_{\max}$ is the maximum intensity of the correlation output, while $E\{I(i,j)\}$ is the mean of the correlation intensity. If the target matches the compressed reference, the correlation function has a sharp peak, and its standard deviation is small. Thus, the PCD is large. If it does not match, the correlation output is broad and its peak is low. Since the standard deviation is large, the PCD is small. In order to compare the recognition performance at the various of the targets screens, each PCD is normalized by the value of the autocorrelation of the noise-free retina image obtained by the conventional JTC.

4.3 Compressed Noise-Free Retina Targets

In order to study the effect of the various compression levels on the recognition performance of the JTC, the noise-free targets were firstly employed. The three-dimensional (3-D) plot of the autocorrelation of the uncompressed retina image is shown in Figure 4.6 (a). The retina recognitions by using the compressed reference with QF = 100 are shown in Figures 4.6 (b), (d) and (f) respectively, while Figures 4.6 (c), (e) and (g) show the results by using the compressed referenced with QF = 10. In Figures 4.6 (b) and (c), the targets were the uncompressed retina images. As a consequence, the correlation peaks are lower and broader than that of the autocorrelation output shown in Figure 4.6 (a). This is caused by the information loss of the compressed reference images. In comparison with Figure 4.6 (c), the

compression of the reference by the QF = 100 gives higher correlation peak as shown in Figure 4.6 (b). It implies that the effect of the reference compression on the retina recognition is significance.

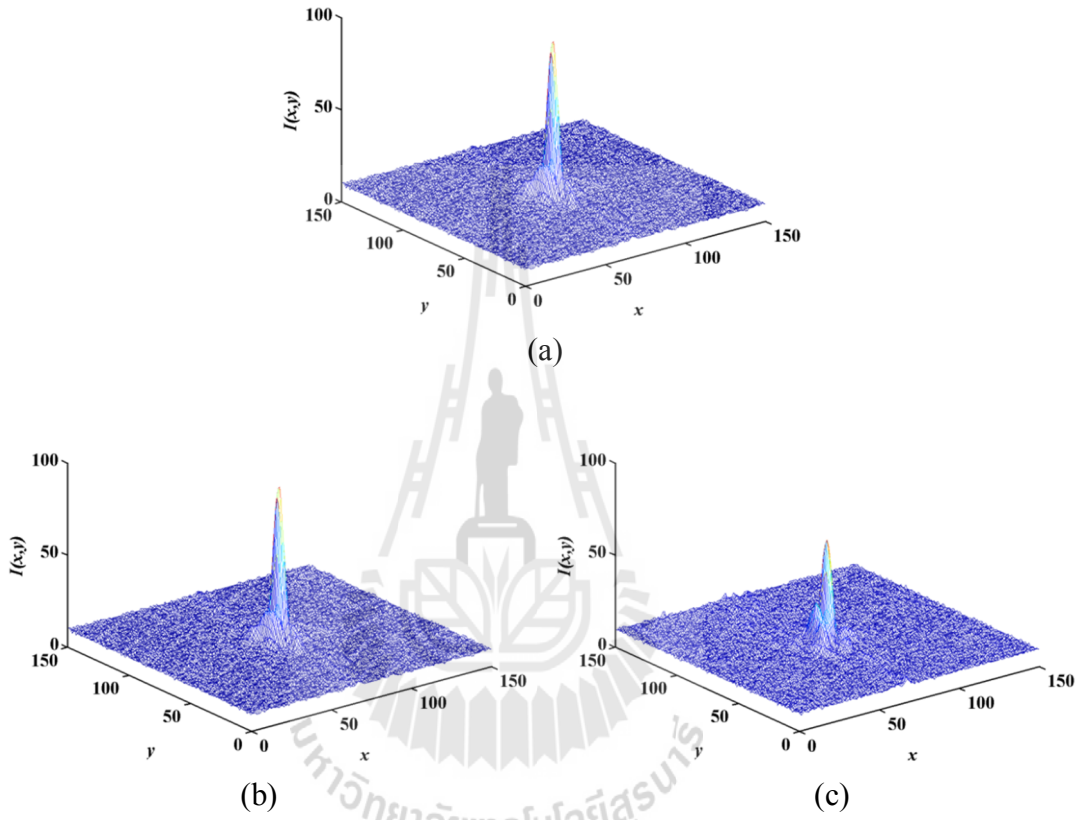

Figure 4.6 Experimental results of the retina detections by using the proposed JTC. (a) Autocorrelation of the uncompressed retina. Cross-correlation outputs of the uncompressed retina target and the reference compressed with QF (b) 100 and (c) 10.

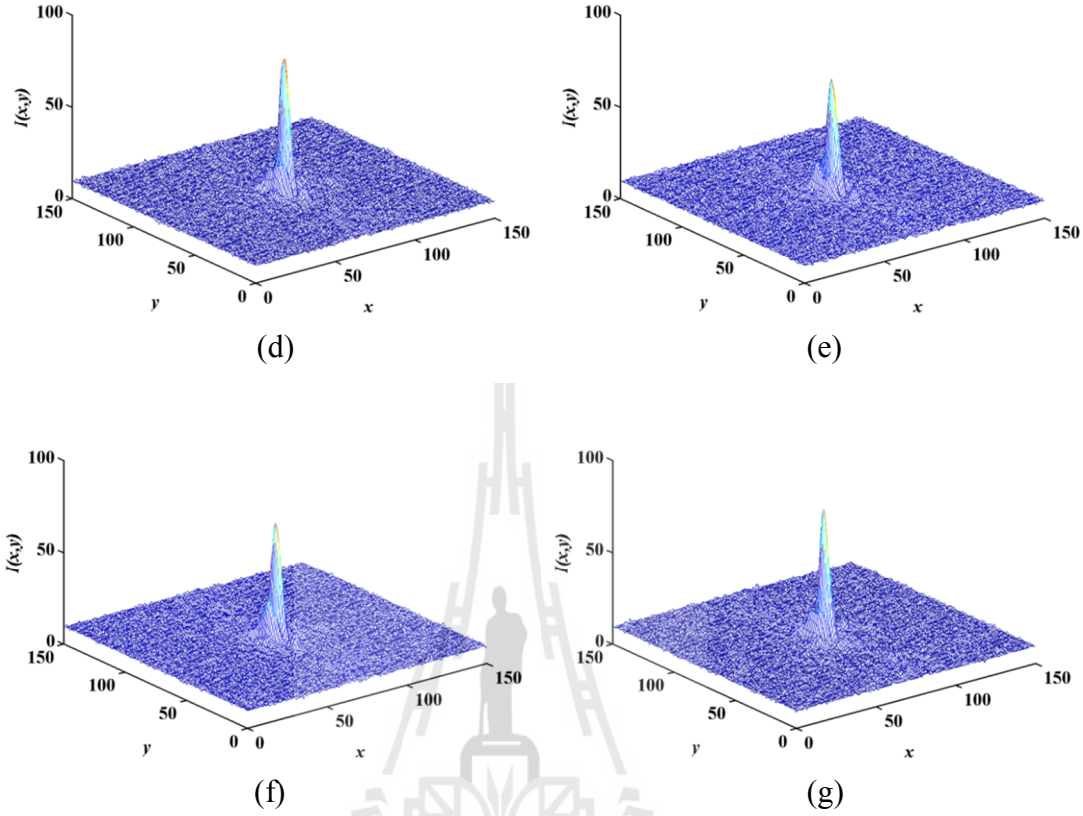

Figure 4.6 (Continued) Cross-correlation outputs of the compressed retina target with QF = 40 and the compressed reference with QF (d) 100 and (e) 10. Cross-correlation outputs of the compressed retina target with QF = 10 and the compressed reference with QF (f) 100 and (g) 10.

In a situation of the retina target was compressed with the QF = 40, the correlation peak obtained by using the retina reference compressed with the QF = 100 is higher than that compressed with the QF = 10 as shown in Figures 4.6 (d) and (e), respectively. Furthermore, when the retina target is compressed with the QF = 10 and the reference compressed with the QF = 10 shown in Figure 4.6 (g), the target matches to the reference. The autocorrelation of the compressed retina occurs. The correlation peak reduces slightly in comparison with the autocorrelation of the uncompressed

noise-free retina shown in Figure 4.6 (a). However, it is higher than Figure 4.6 (f) which corresponds to the cross-correlation operation with the reference compressed with the QF = 100. Therefore, the experimental results show that the retina recognition can be implemented although the target and the reference images are both compressed.

Figure 4.7 shows the variation of the normalized PCDs as a function of the QF of the compressed reference for different target compressions. The normalization is done by using the PCD of the autocorrelation of the uncompressed noise-free retina image. It can be seen that the normalized PCDs of the uncompressed retina target become gradually higher as the QF of the reference image increases. This is because the degree of similarity between the target and reference images becomes higher.

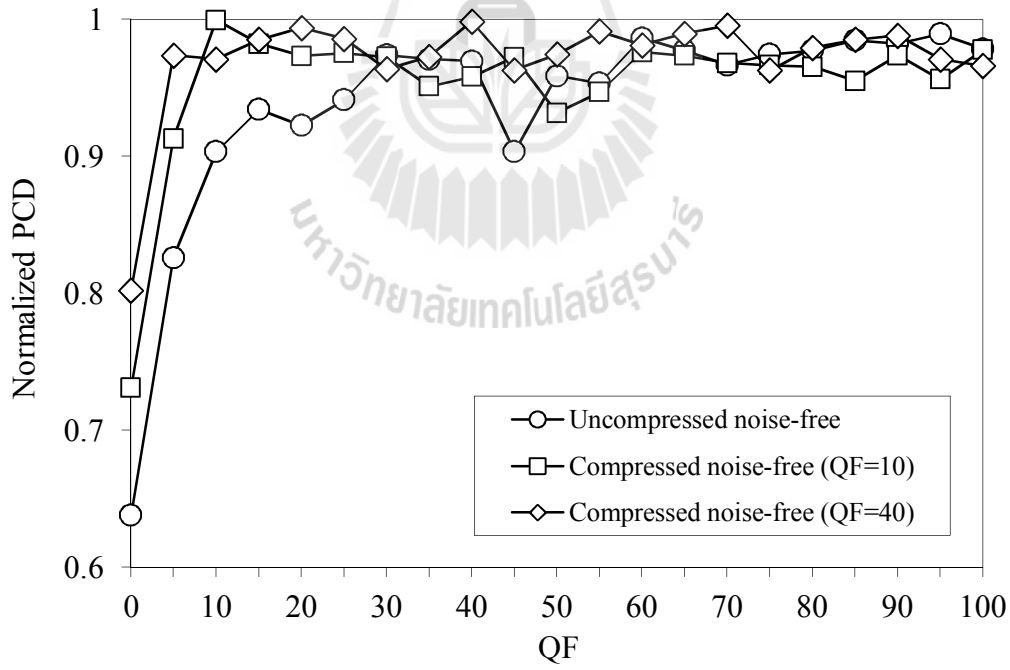

Figure 4.7 The normalized PCD of the noise-free retina recognition as function of the QF of the compressed retina reference for different compression of the targets.

When the target is compressed with the QF = 10, its normalized PCD reaches maximum at the QF = 10, because the target and the reference retina images are identical. For the same reason, the PCD of the compressed target (QF = 40) has a maximum at the QF = 40. However, the PCDs of the compressed noise-free target with the QF = 40 is slightly higher than that of the compressed noise-free with the QF = 10. The reason for this is that the effect of the target compression with the QF = 40 is less severe than that of the QF = 10.

4.4 Compressed Retina Targets Corrupted By Weak Noise

Figures 4.8 (a) – (f) show the 3D recognition outputs of the retina target corrupted by the weak noise with variance $\sigma^2 = 0.01$. Figures 4.8 (a), (c) and (e) corresponds to the retina recognitions by using the references compressed with the QF = 100, while Figures 4.8 (b), (d) and (f) is for the QF = 10. The experimental outputs shown in Figures 4.8 (a) and (b) show that besides the noisy correlation planes, the use of the reference compressed at the QF = 10 gives lower and broader correlation peak intensity than that of the QF = 100. This is because its information loss is more severe. When the noisy retina target is compressed with the QF = 40, the correlation peaks shown in Figures 4.8 (c) and (d) become higher than those in Figures 4.8 (a) and (b), respectively, while the noise in the correlation planes reduces. This shows that the JPEG compression discards not only high spatial-frequency components of the retina image but also that of the noise. As a consequence, besides reducing the target file size, the compression simultaneously suppresses the noise. As the noise degradation corresponding to the second term of Eq. (4.5) reduces, the desired correlation peak increases.

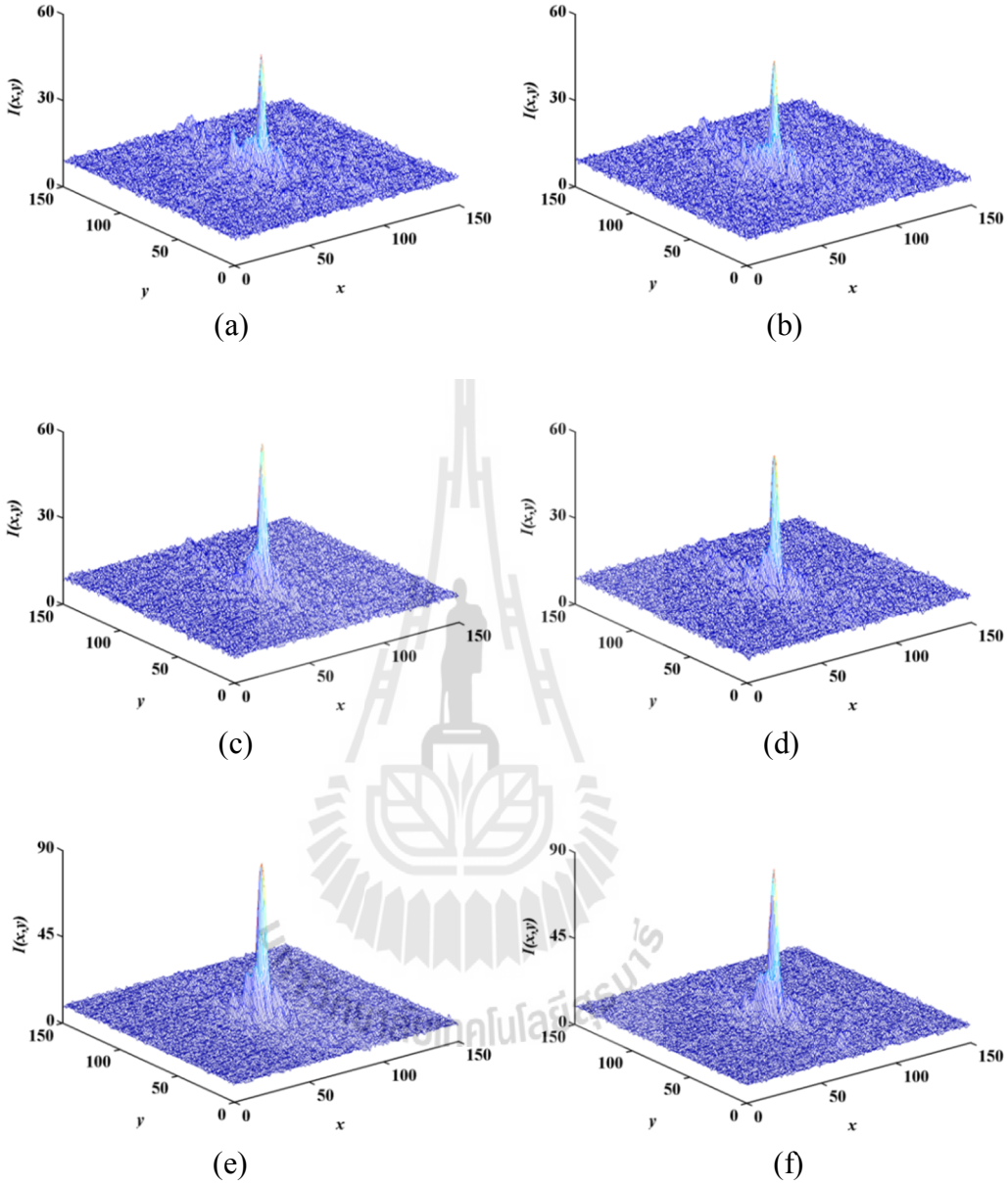

Figure 4.8 Experimental cross-correlation outputs of the uncompressed retina target corrupted by the weak noise (σ^2 = 0.01) and the reference compressed with QF (a) 100 and (b) 10. Cross-correlation outputs of the same noisy retina target compressed with QF = 40 and the reference compressed with QF (c) 100 and (d) 10. Cross-correlation outputs of the same noisy target compressed with QF = 10 and the reference compressed with QF (e) 100 and (f) 10.

However, although the noise can effectively suppressed by using the compression quality QF = 10, information loss of the target becomes more severe than obtained by the QF = 40. Therefore, the corresponding correlation outputs broaden and their peaks increase.

Figure 4.9 shows the normalized PCDs of the noisy retina recognition as a function of the QF of the compressed reference for different target compressions. It is clear that the recognition performance of the CBJTC can be improved by the compressing the noisy targets with the compression QF = 40. It is important to note that the improved PCDs are almost equal to that of the autocorrelation generated by the classical JTC.

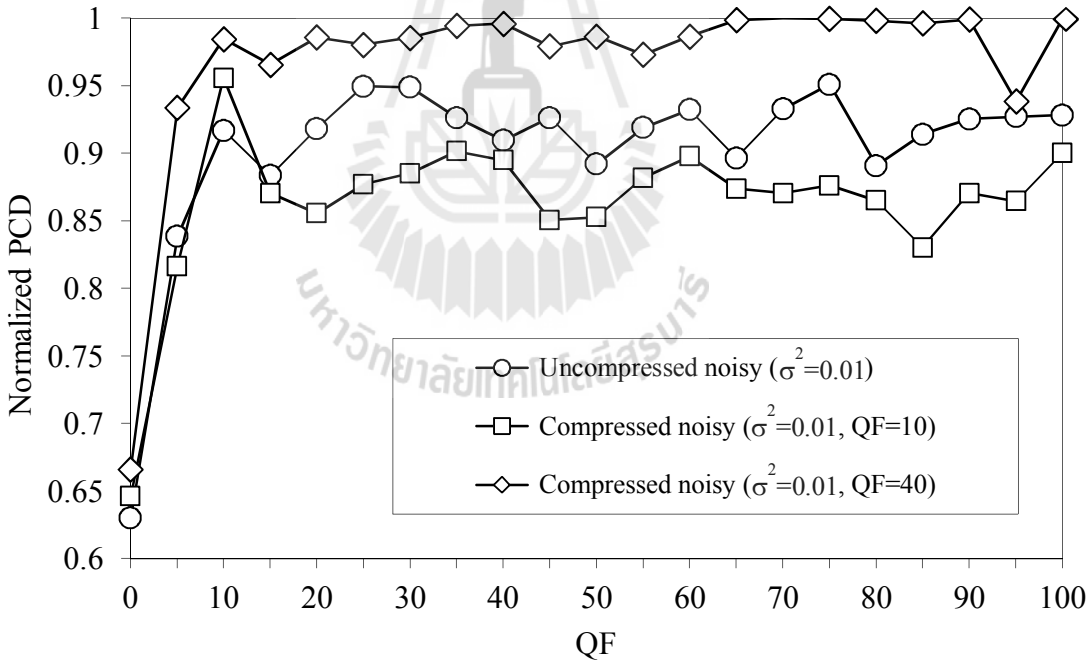

Figure 4.9 The normalized PCDs of the noisy retina recognition (σ^2 = 0.01) as a function of the QF of the compressed reference for different compression of the targets.

As the QF of the compressed reference images becomes smaller, information loss of the reference increases, lowering the PCDs. In accordance with the correlation results shown in Figures 4.8 (e) and (f), the correlation peaks generated by the compressing target with the QF = 10 broaden. Therefore, the corresponding PCDs are lower than the others. In summary, the improved recognition performance verifies that the noise suppression of the retina recognition can be achieved by compressing target images at the appropriate QF.

4.5 Compressed Retina Targets Corrupted By Strong Noise

The experimental output correlations of the retina target corrupted by the noise σ^2 = 1are shown as 3D plot in Figure 4.10. They were generated by using the same references compressed with the QF = 100 and 10. Figsure 4.10 (a) and (b) shows the recognition outputs of the noisy target without the compression. The correlation peaks are hard to be observed, because the second term of Eq. (2.12) degrades severely the desired correlation term. Therefore, when the noisy target is compressed with the QF = 40, the correlation peaks shown in Figures 4.10 (c) and (d) emerge as a result of the noise suppression. However, due to the severe noise degradation, their peak intensities are much lower than those shown in Figure 4.8. When the retina reference is compressed with the smaller QF, the dissimilarity between the target and the reference widens. Consequently, the cross-correlation peak shown in Figure 4.10 (d) broadens and is lower than that in Figure 4.10 (c). Figures 4.10 (e) and (f) show that the improvement of the recognition performance obtained by compressing the noisy target with the QF = 10.

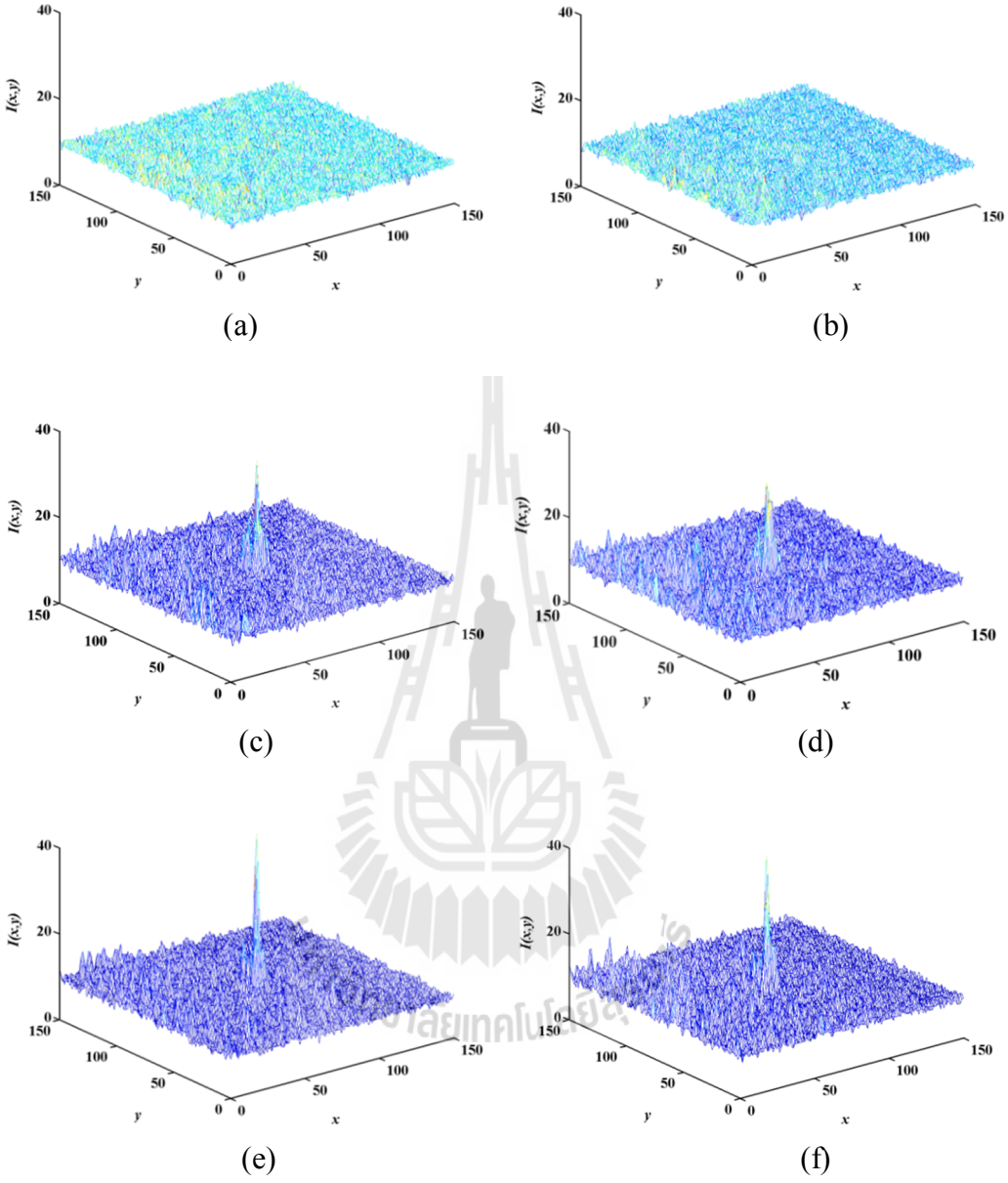

Figure 4.10 Experimental cross-correlation outputs of the uncompressed retina target corrupted by the strong noise (σ^2 = 1) and the reference compressed with QF (a) 100 and (b) 10. Cross-correlation outputs of the same noisy target compressed with QF = 40 and the reference compressed with QF (c) 100 and (d) 10. Cross-correlation outputs of the same noisy target compressed with QF = 10 and the reference compressed with QF (e) 100 and (f) 10.

The correlation peaks are higher than those obtained by the compression with the QF = 40. This reveals that the noise can be further suppressed by using the compression with the QF = 10. This can be understood in terms of spatial-frequency components of the strong noise which is higher than that of the weak noise. To suppress this noise, the compression of the target with smaller QF is required.

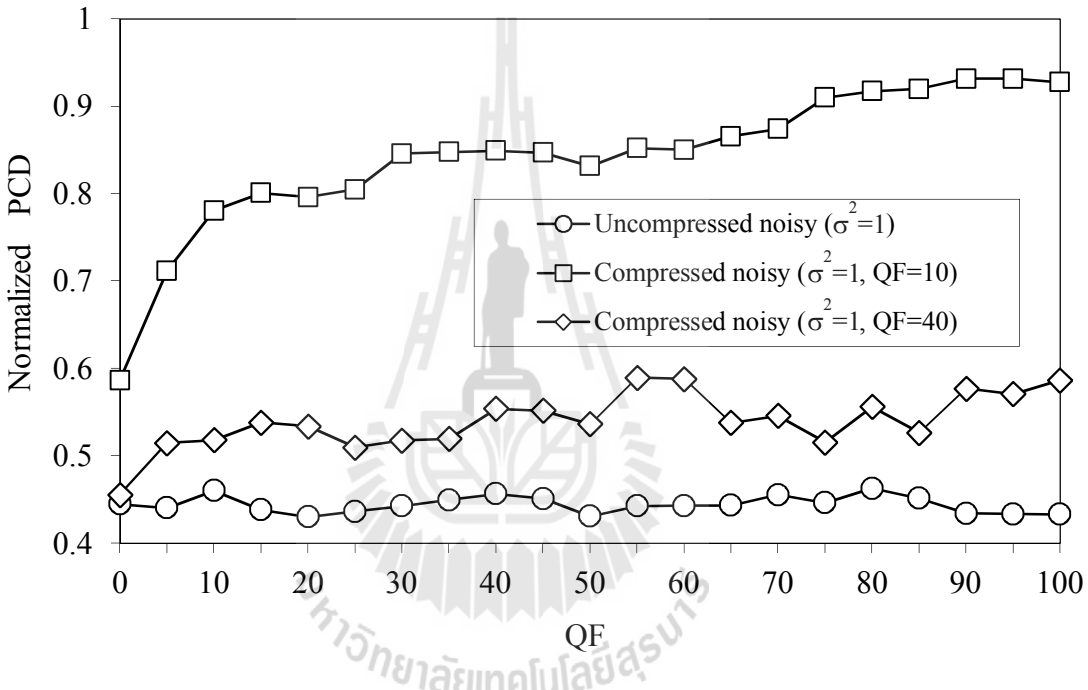

Figure 4.11 The normalized PCDs of the noisy retina recognition ($\sigma^2 = 1$) as a function of the QF of the compressed reference for different compression of the targets.

Figure 4.11 shows the normalized PCD of the recognition of the retina target corrupted by the noise as a function of the QF of the compressed reference for different QF of the target. When the target is not compressed, its normalized PCD is very low of about 0.4 and is almost constant with respect to the QF of the reference.

This is in agreement with the correlation outputs shown in Figures 4.10 (a) and (b) whose peaks are buried in the noise. As a result of the noise suppressions by the target compression, the recognition performance can be improved. In contrast to the previous result, the compression with the QF = 10 gives higher PCDs, because its ability to discard effectively higher spatial-frequency contents of the noise. Therefore, regardless of the noisy level, the compression of the noisy target with appropriate quality can improve the recognition performance of the CBJTC.

CHAPTER V

JOINT-WAVELET TRANSFORM CORRELATOR

In order to improve the retina recognition performance, the CBJWTC is developed by incorporating the WT into the CBTC. In the CBJWTC, a set of wavelet filters generated from the Mexican-hat wavelet function is used to modulate the JPS. As a result of spectral localization, better correlation performance can be produced. The optical implementation of the retina recognition by using the CBJWTC is discussed in Sect. 5.1, while its experimental verifications are presented in Sect. 5.2.

5.1 Optical Implementation of the CBJWTC

A schematic diagram of an optical setup for implementing the retina recognition by using the CBJWTC is the same as the one shown in Figure 4.1. The JPEG-compressed references $r_C(x,y)$ and a set of the dilated filters are stored in a computer system. The JPS of the compressed-retina target $t_C(x,y)$ and reference $r_C(x,y)$ given by

$$\begin{aligned}|G(u,v)|^2 &= \left|R_C(u,v)\exp(-j2\pi x_0 u)+T_C(u,v)\exp(j2\pi x_0 u)+N_C(u,v)\exp(j2\pi x_0 u)\right|^2 \\ &= |R_C(u,v)|^2+|T_C(u,v)|^2+|N_C(u,v)|^2+T_C^*(u,v)N_C(u,v)+T_C(u,v)N_C^*(u,v) \\ &\quad + R_C(u,v)T_C^*(u,v)\exp(-j4\pi x_0 u)+T_C(u,v)R_C^*(u,v)\exp(j4\pi x_0 u) \\ &\quad + R_C(u,v)N_C^*(u,v)\exp(-j4\pi x_0 u)+N_C(u,v)R_C^*(u,v)\exp(j4\pi x_0 u). \end{aligned} \quad (5.1)$$

Is digitally modulated by the Mexican hat filter $\left|H(a_x u, a_y v)\right|^2$. The modified JPS becomes

$$\begin{aligned} O(u,v) &= \left|H(a_x u, a_y v)\right|^2 \left|G\ (u,v)\right|^2 \\ &= \left|H(a_x u, a_y v)\right|^2 \{ \left|R_C(u,v)\right|^2 + \left|T_C(u,v)\right|^2 + \left|N_C(u,v)\right|^2 \\ &\quad + T_C^*(u,v)N_C(u,v) + T_C(u,v)N_C^*(u,v) \\ &\quad + R_C(u,v)T_C^*(u,v)\exp(-j4\pi x_0 u) + T_C(u,v)R_C^*(u,v)\exp(j4\pi x_0 u) \\ &\quad + R_C(u,v)N_C^*(u,v)\exp(-j4\pi x_0 u) + N_C(u,v)R_C^*(u,v)\exp(j4\pi x_0 u)\}. \end{aligned} \tag{5.2}$$

By redisplaying the modified JPS onto the EASLM, the Fourier transformation by the lens L_1 gives the wavelet based correlation output at the back focal plane as

$$\begin{aligned} I(a,x,y)\ \alpha\ [&W_{r_C}(a,x,y)\otimes W_{r_C}^*(a,-x,-y) + W_{t_C}(a,x,y)\otimes W_{t_C}^*(a,-x,-y) \\ &+ W_{n_C}(a,x,y)\otimes W_{n_C}^*(a,-x,-y) + W_{t_C}^*(a,-x,-y)\otimes W_{n_C}(a,x,y) \\ &+ W_{t_C}(a,-x,-y)\otimes W_{n_C}^*(a,x,y) \\ &+ W_{r_C}(a,x,y)\otimes W_{t_C}^*(a,-x,-y)\otimes\delta(x-2x_0) \\ &+ W_{t_C}(a,x,y)\otimes W_{r_C}^*(a,-x,-y)\otimes\delta(x+2x_0) \\ &+ W_{r_C}(a,x,y)\otimes W_{n_C}^*(a,-x,-y)\otimes\delta(x-2x_0) \\ &+ W_{n_C}(a,x,y)\otimes W_{r_C}^*(a,-x,-y) * \delta(x+2x_0)], \end{aligned} \tag{5.3}$$

is detected by the CCD camera. Here, $W_{r_C}(a,x,y)$, $W_{t_C}(a,x,y)$ and $W_{n_C}(a,x,y)$ are the WTs of the compressed reference, target and noise, respectively. The last four terms of Eq. (5.3) can be expressed as

$$W_{r_C}(a,x,y)\otimes W_{t_C}(a,x,y)\otimes\delta(x\pm 2x_0) + W_{r_C}(a,x,y)\otimes W_{n_C}(a,x,y)\otimes\delta(x\pm 2x_0). \tag{5.4}$$

The first term of Eq. (5.4) is the desired WT correlation of the compressed reference and the input target. The second one is the unwanted correlation of the compressed reference and the compressed noise. Since the both terms appear at the same position, the desired correlation term may be corrupted by the unwanted term. Equation (5.4) implies that besides dependence upon the image qualities of the compressed reference $r_C(x,y)$, target $t_C(x,y)$ and noise $n_C(x,y)$, the correlation output is determined by the dilation factor a.

5.2 Experimental Verifications

Experimental verifications of the noisy retina recognition were performed by using the wavelet filters generated with MATLAB software. The experimentally generated JPS in Chapter IV was digitally modulated by the wavelet filter $\left|H(a_x u, a_y v)\right|^2$. Figure 5.1 shows the JPS of the noise-free target and the reference which were compressed by the same QF = 10. To have better insight on the effect of the wavelet filter on the high frequency components of the JPS, zero-order spectra of the JPS is subtracted and a binarization is applied to the resultant JPS. Figures 5.1 (a), (b) and (c) show the effect of the wavelet filtering on the JPS by using the dilation factor $a = 1,\ 2$ and 4, respectively. In comparison with the JPS of the same noise-free retina images shown in Figure 4.4, it obvious that when the dilation factor a is unity, the broad high-spatial frequencies of the fringe pattern is enhanced. Whereas, the large dilation factor $a = 4$ causes the enhancement of the narrow band of the low-spatial frequency components. Since this frequency band is narrower than that of the dilation $a = 1$, its impulse response becomes broader. By using this frequency spectral

localization property, the correlation performance of Eq. (5.3) can be improved according to an appropriate dilation. Figure 5.2 shows the variation of the normalized PCDs of the retina target recognition as a function of the wavelet dilation factors. It is apparent that almost all of the normalized PCDs can be optimized by using the single wavelet filter dilated at $a = 2$. Their maximum values are greater than 2. When the dilation factor is smaller or greater than $a = 2,$ the normalized PCDs decreases. This is because these wavelet filters do not enhance the desired edge features of the retina images.

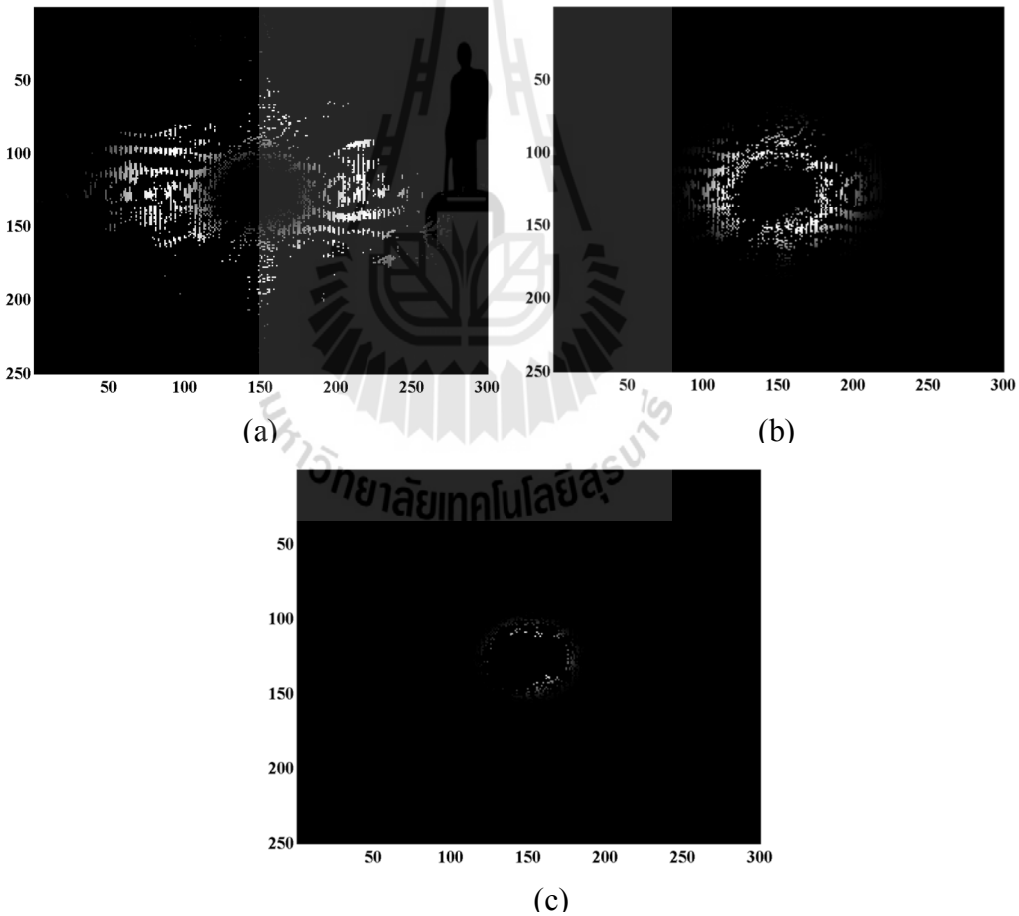

Figure 5.1 The modulated JPS of the compressed noise-free target (QF = 10) and the compressed reference (QF = 10) in situation that the wavelets are dilated at (a) $a = 1,$ (b) $a = 2$ and (c) $a = 4,$ respectively.

The recognition performance of the CBJWTC becomes lower than the classical JTC when the filter dilation increases to be greater than $a = 4$, because according to Figure 5.1 the dilated filter does not localize any fringe information.

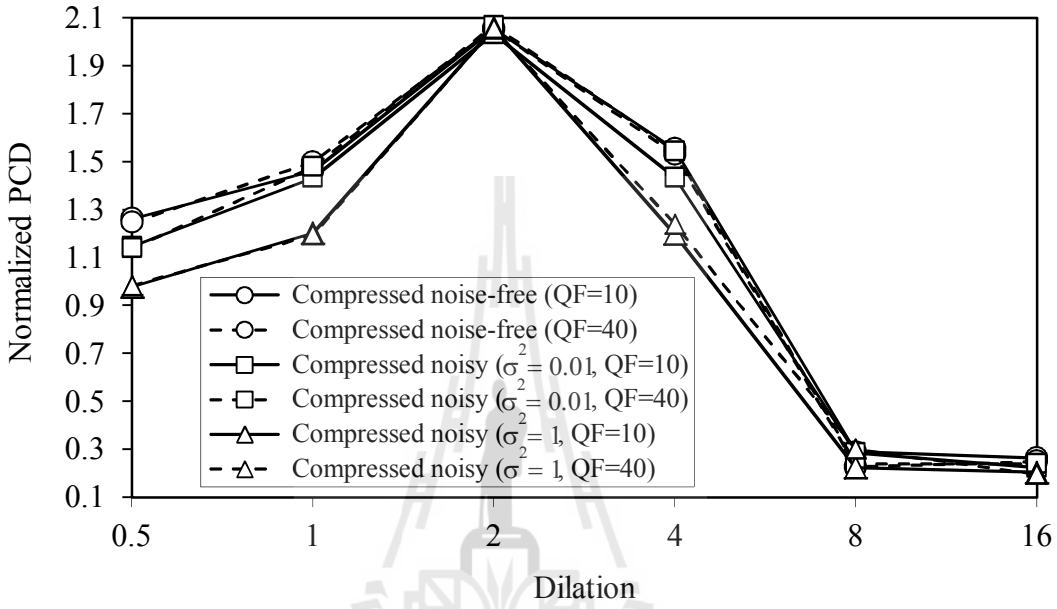

Figure 5.2 Normalized PCDs of the retina recognitions as a function of the dilation factors.

5.2.1 Noise-free retina targets

In Figures 5.3 (a) and (b), the cross-correlation outputs of the compressed noise-free targets with QF = 40 and the reference compressed with the QF = 10 were obtained by using the wavelet filters dilated at $a = 2$ and $a = 4$, respectively. In comparison with the correlation output obtained by using the CBJTC shown in Figure 4.6, the recognition of the proposed method gives higher and sharper correlation intensity peaks. This result also shows that due to the dilation effect, the correlation peak intensity in Figure 5.3 (a) is higher and sharper than that Figure 5.3 (b). In the case of the small dilation factor $a = 2$ which gives the filter with high

center frequency, the high spatial frequency components of the JPS are localized. As a result, the desired features of the retina images such as edges are enhanced, yielding a sharp correlation peak. In contrast, the large dilation factor $a = 4$ causes the filter with a lower center frequency and narrower bandwidth. Since less frequency component of the JPS is enhanced, this filter produces lower and broader correlation peak. Figures 5.3 (c) and (d) show the 3D correlation outputs of the compressed retina targets (QF = 10) by using the same compressed reference and the wavelet filters. In comparison with the Figures 5.3 (a) and (b), the correlation peaks shown in Figures 5.3 (c) and (d) are slightly higher. This is caused by the fact that the target matches to the reference which corresponds to the autocorrelation of the compressed retina images with the QF = 10. The normalized PCDs of the compressed noise-free retina recognitions obtained by using the CBJWTC as a function of the QF of the compressed reference for the different dilation factors is shown in Figure 5.4. It can be seen that the normalized PCDs of the compressed retina target detection by using the wavelet filters dilated at $a = 1,\ 2$ and 4 become greater than 1 for the whole compression quality of the reference images. It obvious that when the dilation factor $a = 2$, the normalized PCDs can be optimized to be higher than 2, regardless of the compression QFs. As shown in Figure 5.2, the other dilation factors give lower PCDs. It is important to note that the dilation $a = 1$ has lower PCDs than $a = 4$. This is because the retina images contain mainly low frequency components. Therefore, unlike the dilation factor $a = 4$, there is no high-frequency spectral enhancement by the wavelet filter dilated at $a = 1$. Furthermore, it can be seen that for the wavelet dilation factor $a = 4$ the normalized PCDs of the noise-free target compressed with the QF = 40 is slightly higher than that compressed with the QF = 10. This is because the target compression with the

QF = 40 contains more high-spatial frequency components than that of the compressed with QF = 10. This is implies that the detections are still dependent upon the compression of the retina target.

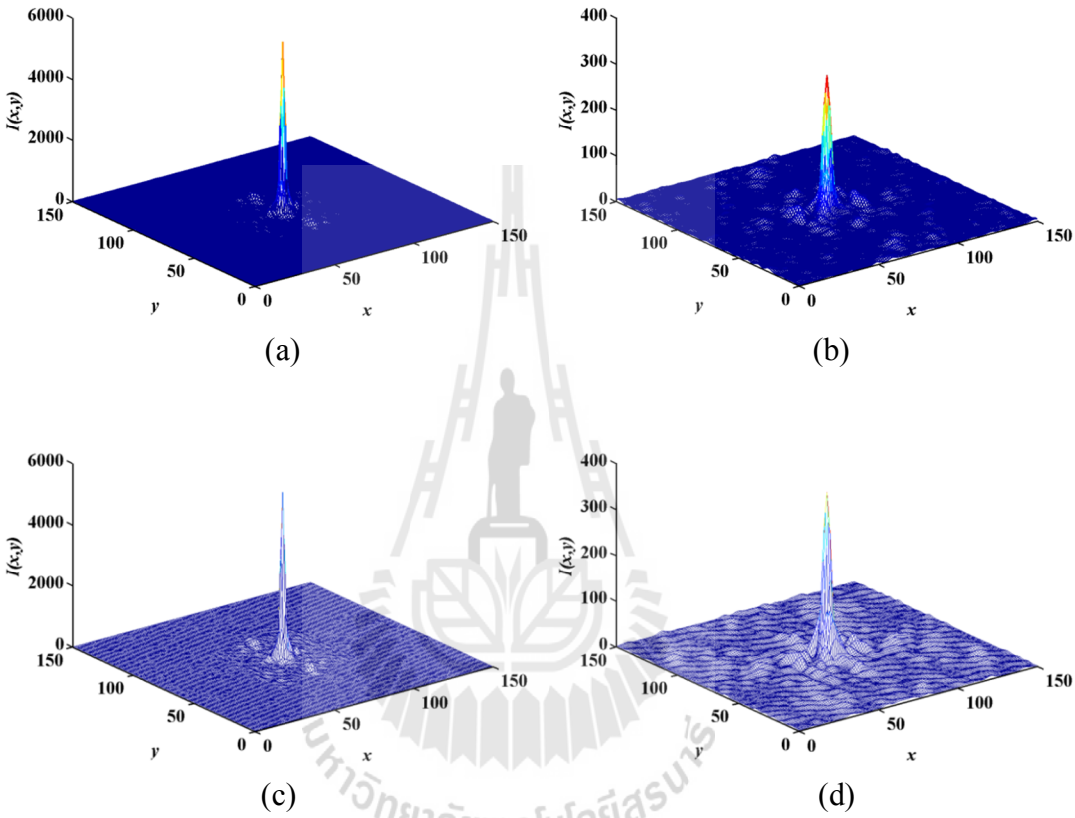

Figure 5.3 3D retina recognition outputs obtained by using the CBJWTC. Cross-correlation outputs of the compressed retina targets (QF = 40) and the compressed reference (QF = 10) in situation that the wavelets are dilated at (a) $a = 2$ and (b) $a = 4$, respectively. Auto-correlation outputs of the compressed targets (QF = 10) and the same compressed reference obtained by the wavelets dilated at (c) $a = 2$ and (d) $a = 4$, respectively.

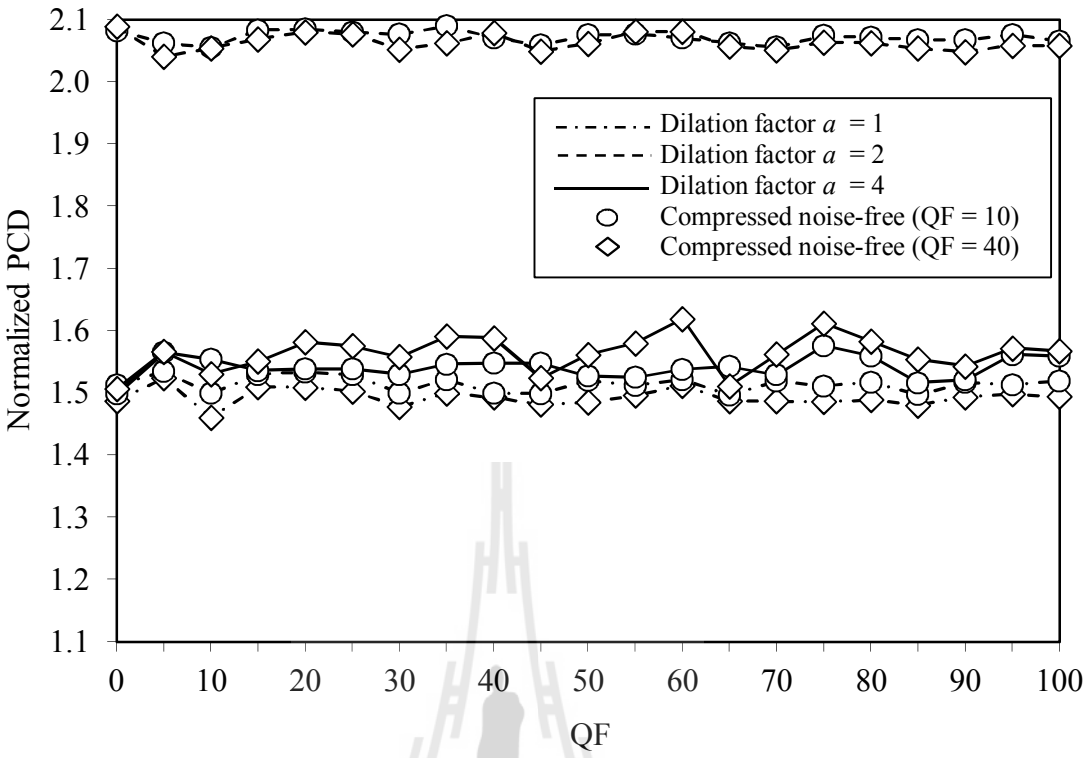

Figure 5.4 The normalized PCDs of the compressed retina target detection (QF = 10) as a function of the QF of the compressed reference for different dilation factors.

In summary, the noise-free retina recognition by using the CBJWTC has better recognition performance than the conventional JTC for the whole compression quality QF. Thus, the dependency of its recognition performance on the reference compression is minimized.

5.2.2 Retina targets corrupted by weak noise

Figure 5.5 shows the 3D recognition outputs of the compressed retina targets corrupted by the weak noise with variance $\sigma^2 = 0.01$. The reference and the target are compressed with the QF = 10 and 40, respectively. In Figures 5.5 (a) and (b), the

cross-correlations were preprocessed by using the wavelet filter with the dilation factors $a = 2$ and $a = 4,$ respectively. While the recognitions of the noisy targets compressed with the QF = 10 and preprocessed by using the same wavelet filters are shown in Figure 5.5 (c) and (d), respectively. It can be clearly seen that the correlation peaks of the retina target corrupted by weak noise ($\sigma^2 = 0.01$) are higher and sharper than those of the CBJTC shown in Figure 4.8. This is because the wavelet filter can enhance the desired high spatial frequency components the compressed target and reference images. Due to its higher center frequency, the use of the wavelet filter dilated at $a = 2$ gives higher and sharper correlation intensities peak than those by the wavelet filter dilated at $a = 4.$ Finally, for the same dilation factor the compression of the noisy targets by using the QF = 40 causes higher correlation peak and less noise in the correlation plane. This is in agreement with the noise suppression results discussed in Chapter IV.

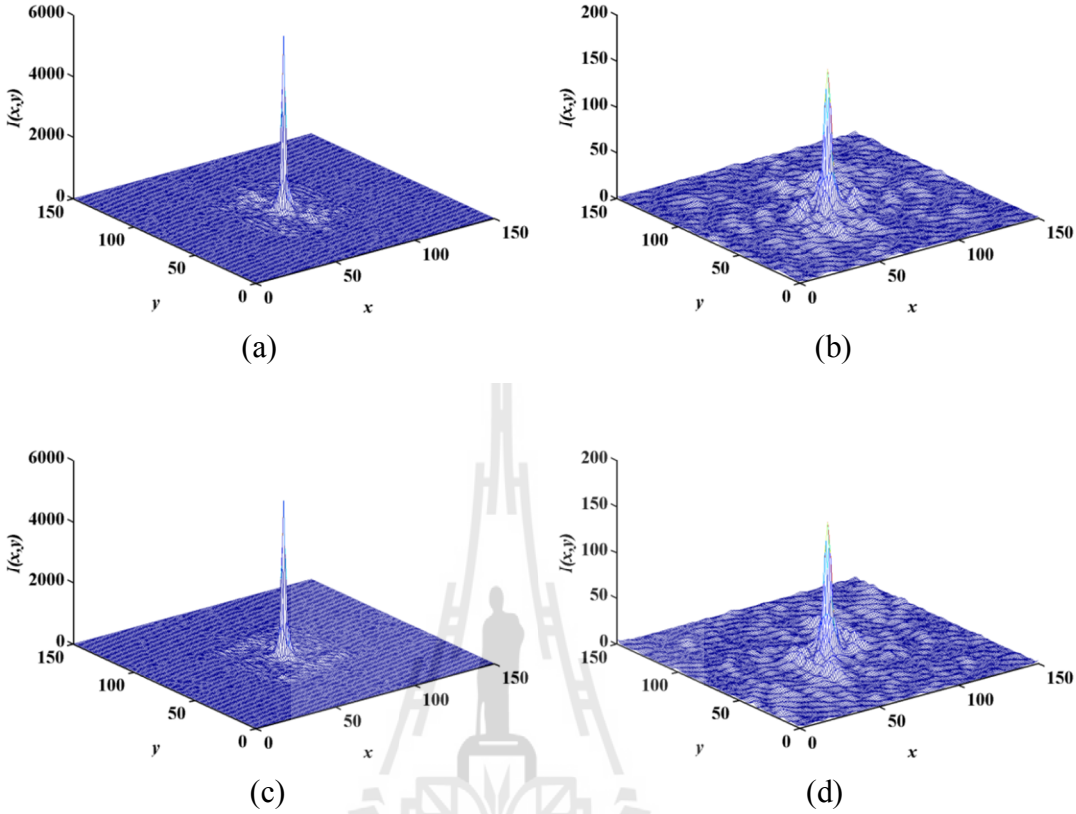

Figure 5.5 3D retina recognition outputs obtained by using the CBJWTC. Cross-correlation outputs of the compressed target corrupted by weak noise ($\sigma^2 = 0.01$, QF = 40) and the compressed reference (QF = 10) in situation that the wavelets are dilated at (a) $a = 2$ and (b) $a = 4$, respectively. Cross-correlation outputs of the compressed targets (QF = 10) and the same compressed reference obtained by the wavelets dilated at (c) $a = 2$ and (d) $a = 4$, respectively.

The normalized PCDs of the noisy target recognitions by using the CBWJTC as a function of the QF of the compressed retina references are shown in Figure 5.6. It can be clearly seen that the normalized PCDs are always greater than 1. Its maximum

value is slightly smaller than 2.1 when the wavelet is dilated with the actor $a = 2$. Since this is the dilation factor which can enhance the desired feature of the retina images, the other dilation factors gives less significant improvement for the whole compression quality QF.

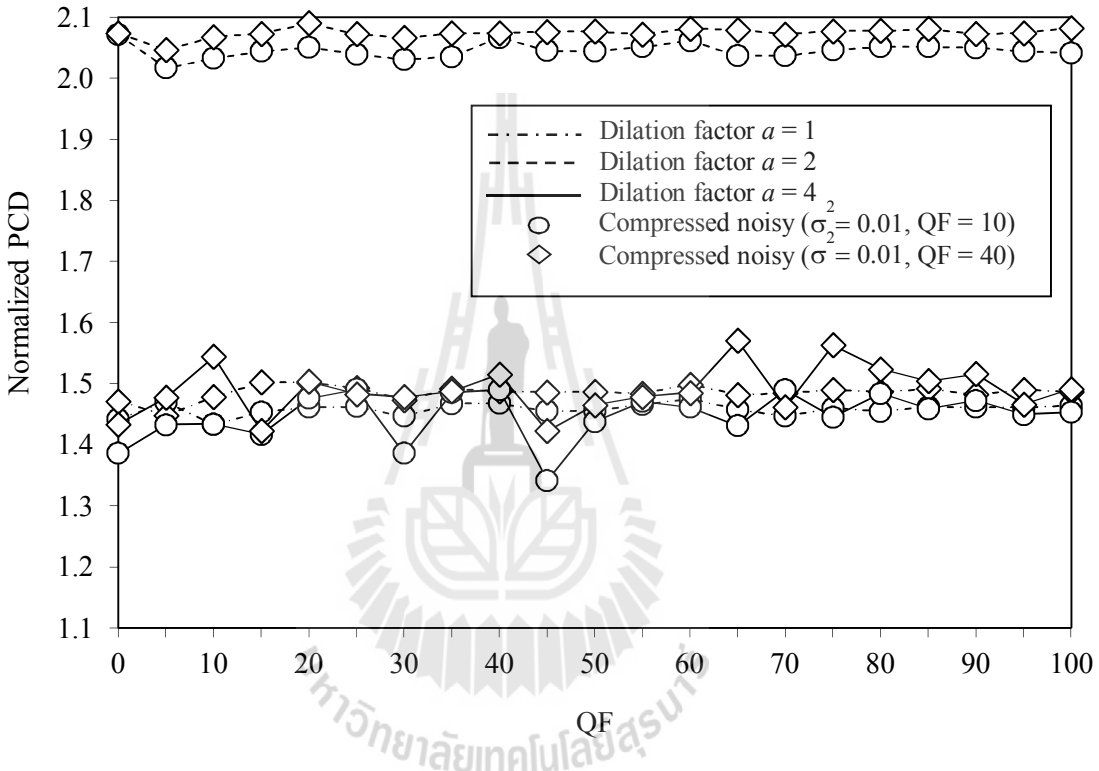

Figure 5.6 The normalized PCDs of the retina targets corrupted by the weak noise with variance $\sigma^2 = 0.01$ as a function of the QF of the compressed reference for different dilation factors.

In comparison with the noise-free retina recognition obtained by using the CBJWTC, the normalized PCDs are slightly lower due to the presence of the weak noise. This corresponds to the contribution of the second correlation term of Eq. (5.3.) While the effect of the noise suppression done by compressing the target with the

QF = 40 can be clearly observed when the dilation factor $a = 2$. This verifies that the JPEG compression can discard the frequency components of the additive noise.

In summary, the CBJWTC can improve the recognition of the retina target corrupted by the weak noise. The wavelet filter dilated at $a = 2$ can be used to optimize the recognition performance. For the same dilation factor, the compression of the noisy target with the QF = 40 can suppress significantly the noise.

5.2.3 Retina targets corrupted by strong noise

Figure 5.7 shows the 3D plot of the recognition outputs of the compressed retina targets corrupted by the strong noise with variance $\sigma^2 = 1$. The recognition is done by the same reference compressed with the QF = 10 and the same dilation factors. In Figures 5.7 (a) and (b), the correlation outputs of the noisy targets compressed with the QF = 40 were obtained by using the wavelet filter dilated at $a = 2$ and $a = 4$, respectively. While Figures 5.7 (c) and (d) correspond to the recognition of the noisy targets compressed with the QF = 10. It can be seen that the correlation peak intensities obtained by using the wavelet filter dilated at $a = 2$ shown in Figures 5.7 (a) and (c) are higher and sharper than those of the dilation $a = 4$ shown in Figures 5.7 (b) and (d). This is in agreement with the results of the noise-free and the noisy ($\sigma^2 = 0.01$) retina target recognitions discussed in Sects. 5.2.1 and 5.2.2, respectively. Although Figures 5.7 (a) and (b) show that the correlation peaks are higher than that Figures 5.7 (c) and (d), the noises in their correlation planes are also higher. This is because the JPEG compression of the target with the QF = 40 cannot suppress effectively the strong noise compared with the QF = 10.

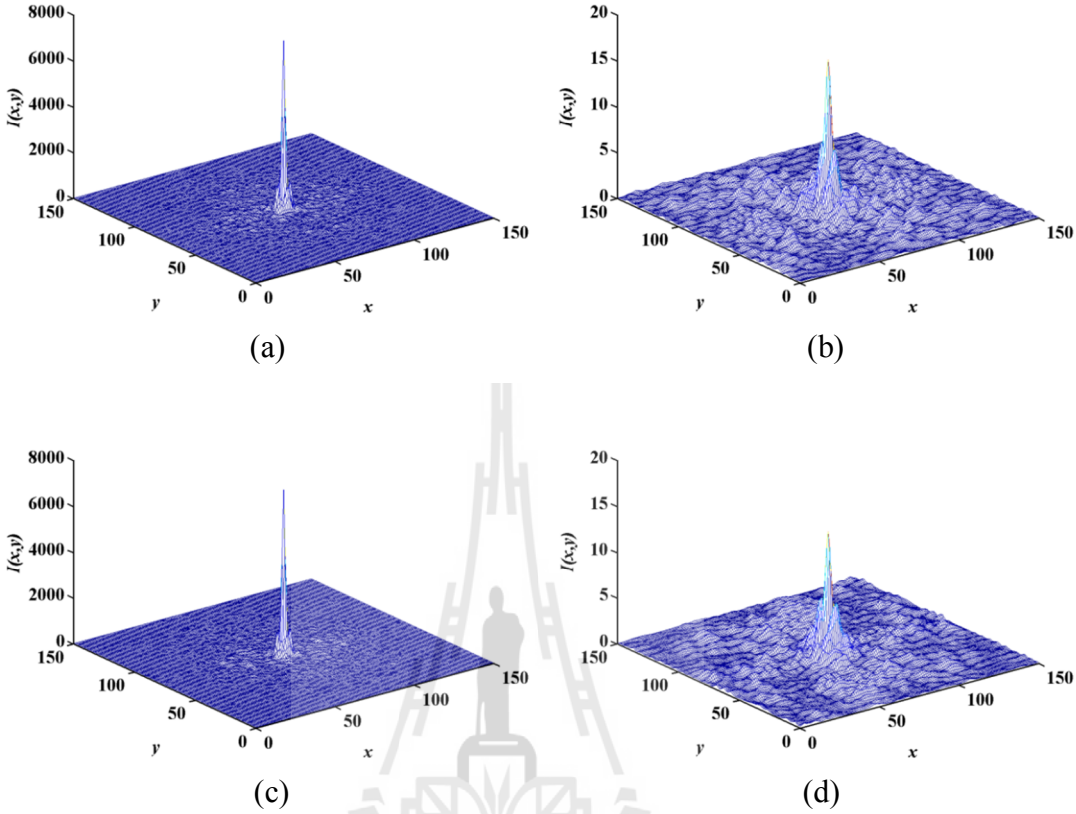

Figure 5.7 3D the retina recognition outputs obtained by using the CBJWTC. Cross-correlation outputs of the compressed the target corrupted by the strong noise ($\sigma^2 = 1$, QF = 40) and the compressed reference (QF = 10) in situation that the wavelets dilated at (a) $a = 2$ and (b) $a = 4$, respectively. Cross-correlation outputs of the compressed retina targets (QF = 10) and the same compressed reference obtained by the wavelets dilated at (c) $a = 2$ and (d) $a = 4$, respectively.

In comparison with the recognition of the retina target corrupted by the weak noise, these correlation peak intensities are higher at the same dilation factor $a = 2$.

This may be caused by the presence of high-spatial frequency components of the strong noise which increases the contribution of the second term of Eq. (5.3.)

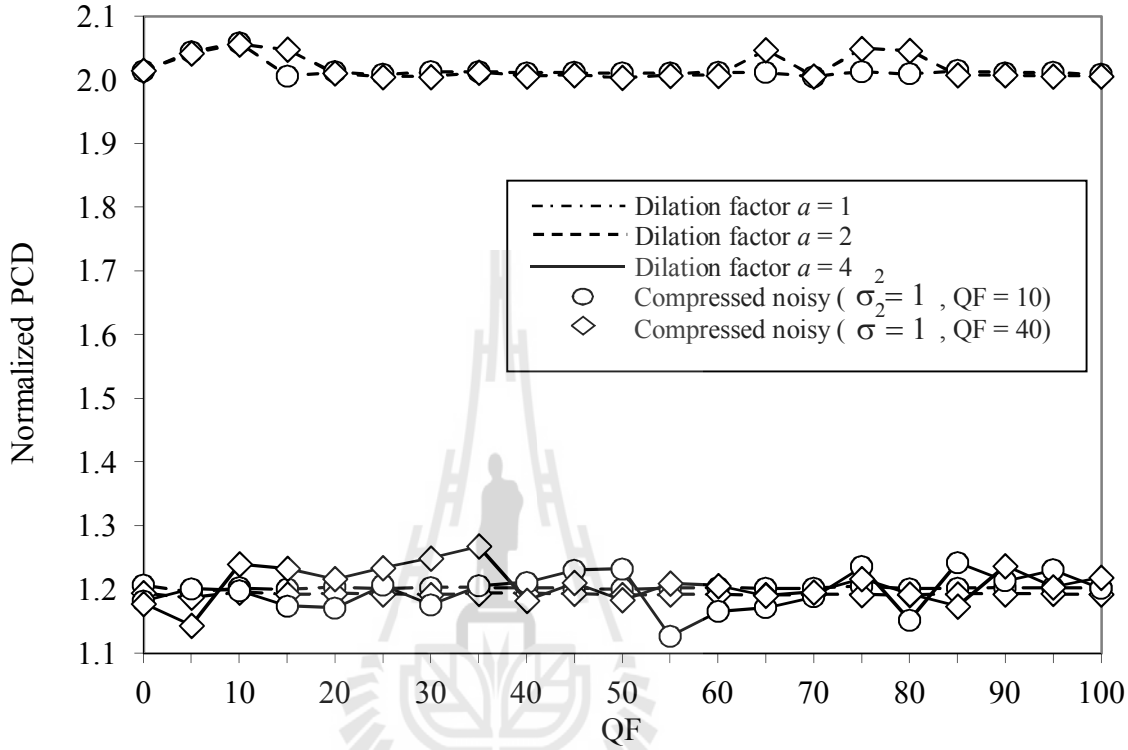

Figure 5.8 The normalized PCDs of the retina targets corrupted by the strong noise with variance $\sigma^2 = 1$ as a function of the QF of the compressed reference for different dilation factors.

Figure 5.8 shows the normalized PCDs of the retina target corrupted by the strong noise as a function of the compressed reference QF for different dilation factors. It is obvious that although the retina target is corrupted by the strong noise, the wavelet filter can still improve the recognition performance for the whole compression quality. As a consequence, the maximum normalized PCDs reduce to about 2 when the dilation factor *a* equals to 2. Although the other dilation factors give lower values,

they are still greater than unity. This verifies that the retina recognition by using the CBJWTC is robust to the noise. For the dilation $a = 2,$ the difference between the PCDs obtained by compressing the retina target with the QF = 40 and 10 becomes smaller. This is because the compression with the QF = 40 cannot suppress the noise as effective as the QF = 10. Consequently, its PCDs decrease. On the contrary, the PCDs due to the compression with the QF = 10 becomes higher. Thus, their differences become smaller.

In summary, the CBJWTC can improve the recognition of the retina target corrupted by the strong noise ($\sigma^2 = 1$). The use of the wavelet filter with the dilation factor $a = 2$ can maximize the recognition performance for the whole compression quality of the reference images. Regardless of the noise level, the CBJWTC performance is always better than the conventional JTC.

CHAPTER VI

CONCLUSIONS

In this thesis work, the retina recognition by using the CBJTC has been experimentally studied. The first part of the work studied the effects of the JPEG image compression on the noisy retina recognition, whereas the second part proposed the improvement of the retina recognition by incorporating the wavelet filters into the CBJTC. The work was done by recording retina images using the non-mydriatic auto fundus camera (Nidek AFC-210). Different level of Gaussian noise generated by Matlab 6.0 were added to the retina target images. The resultant retina targets were then compressed into the JPEG format by using ACDsee software (The 2000 ACD systems, Ltd.). The recognition performance was quantitatively evaluated by using the normalized PCD. The normalization by using the PCD of the autocorrelation of the noise-free retina image was done in order to compare with the performance of the classical JTC.

In Chapter III, the retina images were compressed into the JPEG format with various compression qualities represented by the QF. The effect of compression on image quality was measured by using the PSNR. The results show that the PSNR reduces as the QF becomes small. This is because more information loss due to the images compression.

In Chapter IV, the noise suppression in the retina recognition by using the CBJTC has been experimentally verified by using target images with different noise

levels. Although the experimental results show that the noise suppression can be done by the JPEG compression of the target, the performance of the retina recognition by using the CBJTC is lower than that of the classical JTC. The optimization of the recognition performance can be obtained by choosing appropriate value of the QF such that the stronger the noise, the smaller the compression QF. It is worth mentioning that in the case of the weak noise suppression, the improved recognition performance can be as high as that of the classical JTC.

In Chapter V, a new method for improving the retina recognition by using the CBJWTC has been proposed and experimentally verified. In the CBJWTC, the JPS was modulated by the wavelet filters dilated at appropriated dilation factor. This corresponds to the correlation of the wavelet-transformed retina target and reference images. The experimental results show that the performance of the retina recognition by using the CBJWTC can be improved, yielding better recognition performance than the conventional JTC for the whole compression quality QF. The use of the wavelet filter with the dilation factor $a = 2$ can maximize the detection performance to be 2 times higher than the classical JTC.

As for future work, we are interested in continuing studies of multiple retina recognition by using the proposed CBJWTC. Instead of sequentially performing single target recognition, simultaneous multiple-recognition offers faster processing time. However, due to limited space-bandwidth product of commercially-available EASLMs, an optical implementation of the multiple retina recognition will be a challenge.

REFERENCES

REFERENCES

Allen, J.B. and Rabiner, L.R. (1977). A unified approach to short-time Fourier analysis and synthesis. **Proc**. **IEEE**. 65: 1558-1564.

Alsamman, A. and Alam, M.S. (2003). Face recognition through pose estimation and fringe-adjusted joint transform correlation. **Opt**. **Eng**. 42: 560-567.

Al-Shaykh, O.K. and Mersereau, R.M. (1998). Lossy compression of noisy images. **IEEE Trans**. **Image Proc**. **7**: 1641-1652.

Basu, A., Kamal, A.D., Illahi, W., Khan, M., Stavrou, P. and Ryder, R.E.J. (2003). Is digital image compression acceptable within diabetic retinopathy screening. **Diabetic Med**. 20: 766-771.

Conrath, J., Erginay, A., Giorgi, R., Lecleire-Collet, A., Vicau, E., Kelin, J-C., Gaudric, A. and Massin, P. (2007). Evaluation of the effect of JPEG and JPEG2000 image compression on the detection of diabetic retinopathy. **Eye** 21: 487-493.

Diabetic Retinopathy: **Causes and Risk Factors**. United States National Library of Medicine. (15 September 2009).

Driggers, W., Pennebaker, B. and Mitchell, J.L. (1993). **JPEG Still Image Data Compression Standard**. New York, VanNostrand Reinhold.

Goodman, J.W. (1996). **Introduction to Fourier Optics (2nd ed.)**. New York, McGraw-Hill.

Hill, R.B. (1999). Retina identification, in Biometrics: Personal Identification. In Jain, A.K., Bolle, and Pankanti, R.S. (eds). **Networked Society** (pp.123-141) Springer, New York.

Jain, A.K., Ross, A. and Prabhakar, S. (2004). An introduction to biometric recognition. **IEEE Trans**. **Circuits and Systems for Video Tech**. 14: 4-20.

Jutamulia, S. (2003). Joint transform correlator. In Driggers. R.G. (ed). **Encyclopedia of Optical Engineering** (pp.984-989). Marcel Dekker, New York.

Kertes, P.J. and Johnson, T.M. (eds). (2007). **Evidence-Based Eye Care**. Lippincott Williams and Wilkins, Philadelphia.

Lugt, A.V. (1964). Signal detection by complex spatial filtering. **IEEE Transactions on Information Theory**. 10: 139-145.

Mallat, S. and Hwang, W.L. (1992). Singularity Detection and Processing with Wavelet. **IEEE Trans**. **Inf**. **Theory**. 38: 617-643.

Mallat, S. and Zhong, S. (1992). Characterization of Signals from Multiscale Edges. **IEEE Trans**. **Patt**. **Anal**. **Machine Intell**. 14: 710-732.

Marr, D. and Hildreth, E. (1980). Theory of edge detection. **Proc**. **R**. **Soc**. **Lond**. **B**. 207: 87-217.

Pennebaker, W.B. and Mitchell, J.L. (1993). **JPEG Still Image Data Compression Standard**. Van Nostrand Reinhold, New York.

Roberge, D. and Sheng, Y. (1994). Optical composite wavelet-matched filters. **Opt**. **Eng**. 33: 2290-2295.

Roberge, D. and Sheng, Y. (1994). Optical wavelet matched filter. **Appl**. **Opt**. 33: 5287-5293.

Salomon, D. (1998). **Data Compression: The Complete Reference**. New York, Springer-Verlag.

Sheng, Y., Roberge, D., Szu, H. and Lu, T. (1993). Optical wavelet matched filters for shift-invariant pattern recognition. **Opt**. **Lett**. 18: 299-301.

Yang, S., Zhang, X. and Mitra, S. (1999). Performance of lossy compression algorithms from statistical and perceptual metrics. In **Proceedings of 12th IEEE symposium on Computer-based Medical Systems**. 242-247 pp.

Young, R.K. (1993). **Wavelet theory and its applications**. Kluwer, Dordrecht.

Yu, F.T.S., Jutamulia, S., Lin, T.W. and Gregory, D.A. (1987). Adaptive real-time pattern recognition using a liquid crystal TV based joint transform correlator. **Appl**. **Opt**. 26: 1370-1372.

Yu, F.T.S. and Lu, X.J. (1984). A real-time programmable joint transform correlator. **Opt**. **Comm**. 52(1): 10-16.

Widjaja, J. (2003). Wavelet transform correlator. In Driggers, R.G. (ed**)**. **Encyclopedia for optical engineering** (pp. 2993-99). Marcel Dekker, New York.

Widjaja, J. (2006). **Optical Target Recognition: Fundamentals and Applications**. Suranaree University of Technology, Nakhon Ratchasima.

Widjaja, J. (2007). Detection performance of wavelet-based joint transform correlation. **Appl**. **Opt**. 46: 8278-8283.

Widjaja, J. (2010). Wavelet filter for improving detection performance of compression-based joint transform correlation. **Appl**. **Opt**. 49: 5768-5776.

Widjaja, J. and Suripon, U. (2004). Real-time joint transform correlator by using compressed reference images. **Opt**. **Eng**. 43: 1737-1745.

Widjaja, J. and Suripon, U. (2005). Multiple-target detection by using joint transform correlator with compressed reference images. **Opt**. **Commun**. 253: 44-55.

Widjaja, J. and Suripon, U. (2006). Experimental verifications of joint transform correlator using compressed reference images. **Appl**. **Opt**. 45: 8074-8082.

Widjaja, J. and suripon, U. (2011). Retina recognition using compression-based joint transform correlator. **Opt**. **Eng**. 50(9): 98-201.

Widjaja, J. and Kaewphaluk, K. (2014). Experimental verifications of noise suppression in retinal recognition by using compression-based joint transform correlator. **Opt**. **Commun**. 315: 188-192.

CURRICULUM VITAE

Mr. Komin Kaewphaluk was born on November 14, 1977 in Bangkok. He received a B.Sc. degree in Physics from Srinakharinwirot University, Prasarnmit in 1999 and his M.Sc. degree in Physics from Chulalongkorn University, Bangkok in 2003. He pursued his Ph.D. degree in Physics from the Suranaree University of Technology. He has one publication entitled "Experimental verifications of noise suppression in retinal recognition by using compression-based joint transform correlator", published in Optics Communications 2014. He is working as a teacher in Department of Physics at Chulachomklao Royal Military Academy. His research of interests includes optical information and image processing.